X-612-66-109

CORRELATIONS OF MAGNETIC FIELDS AND ENERGETIC ELECTRONS ON THE IMP-I SATELLITE

BY

K. A. ANDERSON
N. F. NESS

MARCH 1966

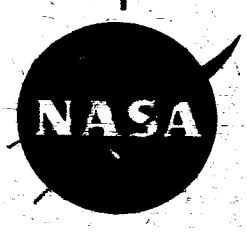

GODDARD SPACE FLIGHT CENTER
GREENBELT, MARYLAND

CORRELATIONS OF MAGNETIC FIELDS AND ENERGETIC ELECTRONS ON THE IMP-1 SATELLITE

by

K. A. Anderson
Physics Department and
Space Sciences Laboratory
University of California, Berkeley

and

N. F. Ness
Laboratory for Space Sciences
NASA-Goddard Space Flight Center
Greenbelt, Maryland

March 1966

CORRELATIONS OF MAGNETIC FIELDS AND ENERGETIC ELECTRONS ON THE IMP-1 SATELLITE

K. A. Anderson
Physics Department and
Space Sciences Laboratory
University of California, Berkeley

and

N. F. Ness
Laboratory for Space Sciences
NASA - Goddard Space Flight Center
Greenbelt, Maryland

ABSTRACT

A study of simultaneous magnetic field and energetic particle records from the IMP-1 satellite on the dark side of the earth has shown several distinct correlations which can be understood as diamagnetic effects of charged particle populations. Depression of the magnetic field in the closed magnetic field line configuration of the particle cusp region is observed on most orbits. Attributing this depression to the diamagnetic effects of particles, about 1% of the effect can be attributed to electrons >45 keV. In the geomagnetic tail region, large depressions of the magnetic field having radial extent ~10 R_e are observed when the satellite approaches the neutral sheet to within ~5 R_e. Energetic electron fluxes appear throughout this volume and show no strong preference to occur immediately adjacent to the neutral sheet. In this region, less than 1% of the diamagnetic effect is due to electrons >45 keV. Finally, there are examples of intense, energetic electron fluxes closely associated with reduction of the magnetic field magnitude. In one case an electron flux of 3×10^6 $cm^{-2}sec^{-1}$ >45 keV was associated with a field change from 20γ to 8γ.

Author

INTRODUCTION

The highly eccentric orbit of the IMP-1 satellite has permitted an extensive set of observations of fields, particles and plasmas to be accumulated in the region surrounding the earth out to geocentric distances of 31.7 earth radii (R_e). Of particular interest in connection with terrestrial phenomena has been the nature of the geomagnetic field in the anti-solar direction and the particle populations in that region. Results from the IMP-1 satellite have provided the most complete description of the geomagnetic field on the night side of the earth at distances where the dipole character of the field has been greatly distorted to form a magnetic tail. The field has been shown to have approximately a 40 R_e diameter at a geocentric distance of 30 R_e with the lines of force directed parallel to the earth-sun line. These measurements have also led to the discovery that the night-side geomagnetic field is divided into two great bundles of magnetic lines, pointing directly away from the sun south of the plane of the magnetospheric equator and toward the sun above this plane. These bundles of lines have been shown to be separated by a neutral sheet which is very thin if its thickness is taken to be defined by the angular coordinate specifying direction of the field with respect to the sun-earth line. The observed neutral sheet positions have been shown by Ness (1965) to lie close to the solar-magnetospheric equatorial plane.

Measurements on the Explorer XIV satellite reported by Cahill give considerable information on the region from 6 to 16 R_e that is intermediate between the fully developed geomagnetic tail and

the inner dipole-like region. Of particular interest was the finding that near the plane of the geomagnetic equator at geocentric distances between 8 and 10 R_e a depression in the magnitude of the field occurs. Cahill attributed this effect to a plasma whose high energy tail had been detected in several satellite experiments. The large fluxes of low energy (1-10 keV) particles in this intermediate region have been studied by Gringauz (1960) and by Freeman (1964) and at higher energies (>40 keV) by Frank (1965), by Anderson (1965) and most recently by Serlemitsos (1966). An extensive set of particle measurements in the geomagnetic tail comes from the Vela satellites which have circular orbits of about 17 R_e geocentric radius, close to where Ness (1965) places the beginning of the characteristic tail topology. The most recent published work from the Vela group is authored by Coon (1965) and by Bame, et al (1966). Another set of particle measurements in the geomagnetic tail comes from IMP-1 and thus extends out to geocentric distances of nearly 32 R_e. These measurements were most recently discussed by Anderson (1965). The most significant finding was that fluxes of energetic electrons up to 10^7 $cm^{-2}sec^{-1}$ show an impulsive character. That is, in regions of space several earth radii in extent these particles appear with onset times of 10 to a few hundred seconds, and then decay away with a time constant from several minutes to one hour.

Examples of energetic electron island fluxes may be seen in many of the Figures presented here. Figures 11 and 13 show particularly clear examples. This fast-slow characteristic is observed regardless of whether the satellite is outbound or inbound. These observed changes of counting rate in the Geiger-Mueller tube are due to temporal changes in the energetic electron

flux at a fixed point in space. The motion of the satellite plays only an inconsequential part in changes of the counting rate. Detailed discussion of this point is given in the reference just cited. The definite characteristics of these energetic electron fluxes in the geomagnetic tail require a means of referring to them. They will be referred to as energetic electron islands until their true physical nature is known at which time it will be possible to describe them in terms of basic, causal phenomena.

The present work is an attempt to relate features of the magnetic field to high energy electron fluxes in the geomagnetic tail using results from the IMP-1 satellite. This spacecraft, its orbit and details of the magnetometer instrumentation have been described by Ness, Scearce and Seek (1964). The particle counters have previously been described in detail by Anderson, Harris and Paoli (1965).

This article identifies significant departures from the average or typical field situation in the geomagnetic tail as reported by Ness (1965) and relates these to changes in energetic particle fluxes.

PROCEDURE

In order to identify departures from an idealized geomagnetic tail field static in time and slowly changing in space, the three magnetic field quantities in solar-ecliptic coordinates have been plotted versus a linear scale of geocentric distance along with the counting rate of the Geiger-Mueller tube. These plots, for only the inbound orbital pass, will tend to emphasize spatial effects and somewhat obscure temporal effects but the main purpose of the study is to determine the size of regions in which departure from idealized behavior is found. The procedure is then to make a visual inspection of the combined field and particle records. Here we discuss three types of field-particle correlations:

1. Magnetic field depressions in the particle cusp region
2. Broad magnetic field depressions in the fully developed geomagnetic tail
3. Detailed features of the magnetic field during the appearance of electron island fluxes.

In discussing certain of these features, particularly for comparing one with another, it has been found useful to introduce a quantity R:

$$R = \frac{4\pi(j_{max} - j_{min})}{\frac{1}{2\mu_o}(F_{max}^2 - F_{min}^2)} \cdot E$$

This quantity is calculated for cases of simultaneous field and particle changes. j_{max} is the directional electron intensity >45 keV associated with the magnetic field magnitude F_{max}.

J_{min} is the directional intensity associated with the field F_{min}. $\bar{E}$ is the average energy detected by the IMP-1 particle detector, and v is the velocity corresponding to this energy. In all cases $\bar{E}$ is taken to be 100 keV and the velocity is then 1.6×10^{10} cm/sec. When R changes, part of the change may be due to changes in the spectrum of the particles above 45 keV. However, the variation of $\bar{E}/v$ cannot be very great since this quantity varies approximately as the velocity to the first power.

The directional intensities are assumed to be isotropic over all solid angles so that they can be related to the counting rate in the IMP-1 Geiger-Mueller tube:

$$J = \frac{C}{\epsilon G_1}$$

where C is the counting rate, corrected for dead time effects, due to electrons >45 keV. G_1 is the geometric factor of the entrance collimator geometry. This is calculated as a telescope factor and is found to be $G_1 = 2.5 \times 10^{-2}$ cm^2-sterad. The quantity ϵ is the efficiency for scattering electrons from the gold foil into the active volume of the Geiger-Mueller tube. This has been shown to be energy independent over a wide energy range. The absolute value for this particular geometry is 0.07.

R is used as a dimensionless parameter in an attempt to organize certain features of the field-particle correlations. The quantity $\frac{1}{2\mu_o}(F_{max}^2 - F_{min}^2)$ is a measure of the total particle energy density assuming that pressure by waves is negligible. The quantity $\frac{4\pi\Delta J\bar{E}}{v}$ is simply the energy density

in a given region due to electrons >45 keV since in most cases $j_{max} >> j_{min}$, and hence $\Delta j \approx j_{max}$. Therefore R in most cases gives the ratio of energy density due to energetic electrons to the energy density due to all charged particles of all energies in a given region. In this sense it may be used to indicate the hardness or softness of the particle populations in a given region. If the energy spectrum and the pitch angle distribution of the energetic electrons were known, the partial pressure exerted by these particles could be calculated. This partial pressure is given by:

$$p = \frac{\bar{E}_\perp}{\bar{E}} R$$

$\bar{E}_\perp$ is the average perpendicular energy carried by the electrons >45 keV and $\bar{E}$ is the average total energy carried by them. These quantities are integrals having the form:

$$\bar{E}_\perp = \int \int E \sin\alpha \frac{d^2n(\alpha,E)}{d\alpha dE} d\alpha\, dE$$

$$\bar{E} = \int \int E \frac{d^2n(\alpha,E)}{d\alpha\, dE} d\alpha\, dE$$

The integrals are to be carried out over particles moving in both directions and the energy integrals begin at 45 keV in the present case. The ratio of the two integrals in effect gives an average pitch angle $\overline{\sin\alpha}$. The partial pressure is then:

$$p = \overline{\sin\alpha}\, R \qquad \text{Percent}$$

RESULTS AND DISCUSSION

Inspection of the combined vector magnetic field-energetic electron measurements from the orbits of IMP-1 confined to the geomagnetic tail region show the following main features:

I. Field-particle correlations in the particle cusp region.

On most of the orbits 31 to 47 the field is depressed below its expected value over an extended region corresponding to the specific particle feature in the distant radiation zone variously called the cusp or the particle tail. The cusp is an energetic particle feature on the night side of the earth readily identified on most orbits. It is confined in latitude and shows sudden and large counting rate transition on its outward side. This boundary is usually between 10 and 15 R_e. For example, on orbit 31 (Fig. 1) the flux in the cusp is 1.4 to 2.1 x 10^7 $cm^{-2}sec^{-1}$ from 13 to 14.5 R_e but in less than 0.5 R_e the flux drops to about 1.4 x 10^5 $cm^{-2}sec^{-1}$. Inspection of the combined IMP-1 particle-field records shows that on 10 orbits out of 15 for which complete data records were available the cusp showed a sharp, well-defined transition having a counting rate change of at least a factor of 10. In all but one of these ten cases the magnetic field was observed to decrease abruptly in close association with the particle increase at the cusp boundary. The field and particle changes are simultaneous to within a few minutes or a few hundred kilometers. The changes in the field magnitude associated with the cusp boundary are from 5 to 20γ. Figures 2, 3, 4, 5 and 6 further illustrate this effect. In all these cases, geomagnetic conditions were quiet.

In the case of the other five tail orbits from IMP-1 which permit simultaneous study of fields and particles, a well-defined jump in both particle flux and magnetic field does not occur. In these cases the boundary of the cusp cannot be determined because the fluxes are weak and show no sharp transition. In two or three cases a cusp boundary can be tentatively identified but the magnetic field makes no clearly associated jump. An example of this behavior is shown in Fig. 7. Geomagnetic conditions were very quiet on this occasion.

Table I summarizes the field and particle data for those cases where the cusp region is well developed. In eight of the ten cases, magnetometer data is available and the field magnitudes just inside and just outside the cusp boundary are listed in Table I. The field inside the boundary sometimes fluctuates so that it is necessary to perform some averaging. Several examples of how the values in the table were obtained are given in Figs. 1, 2, 3, 4, 5 and 6. These examples serve to show how well-defined the particle-field association is in many cases and also that any other averaging that may be employed will not greatly change the listed values. The next entry in the table is the ratio R, calculated for the associated field and particle changes across the cusp boundary. The numerical values range from 0.12% up to 4.5%. However, if the lowest value is ignored, the spread is only a factor of 5. The final entry in Table I is the Kp sum for the day preceding the observation. There is some tendency for high Kp sums to go with the higher particle energy to magnetic pressure ratios and for the lowest ratios to be accompanied by low Kp sums.

We next attempt to relate this behavior of the particle population to behavior of the magnetic field lines in this region. The interpretation consists of the following statements:

1. The lines of magnetic force in the particle cusp region, though considerably distorted by comparison with a dipole field, are closed in the vicinity of the earth and particles are able to execute well defined motions between mirror points. Measurements on Explorer XIV (Cahill, 1965) show closure of lines in the vicinity of the earth out to a distance of 14 R_e on one occasion. The energetic electron fluxes in the cusp are often closely the same as the fluxes in the durable trapping region. Recent results published by Serlemitsos (1966) show that in this region energetic electrons have a pitch angle distribution characteristic of their being trapped on lines of force which connect directly one hemisphere with the other.
2. The diamagnetic effects of charged particles trapped on these lines of force are responsible for the reduction of the magnetic field magnitude. This effect is appreciable from the outer boundary of the cusp to 3 - 4 R_e earthward from this boundary. The magnetic field is reduced from 30γ outside its boundary to 15γ inside the boundary in a typical case.
3. The cusp boundary represents the first open line of force. By open is meant that the line of force is at least several times as long as its neighbor on the earthward side. This sudden change will then alter the flux and perhaps other features of the particle population and thereby accounts for the well defined boundary observed in this region.

4. The open lines of force beyond the cusp boundary have different populations of particles, namely those characteristic of the geomagnetic tail region.
5. Assuming wave pressure in the cusp region is not important, the magnetic pressure differential at the outer boundary given by $\frac{1}{2\mu_o}(\bar{F}_{max}^2 - \bar{F}_{min}^2)$ must be balanced by a particle pressure. The ratio R can then be written as $R \sim \frac{u}{U}$. u is $\frac{4\Delta f \bar{E}}{v}$ and U is the kinetic energy density of all charged particle populations in the cusp region. The proportionality results from the fact that the pitch angle distributions of the particles have not been accounted for. R may be interpreted as a measure of relative hardness or softness of the energy spectra in this region: A large value of R means that compared to the particles exerting the pressure against the magnetic field jump the number of energetic electrons is relatively large.

The partial pressure exerted by electrons above >45 keV against the magnetic field can be estimated from a knowledge of pitch angle distributions on the lines of force in the cusp region. The partial pressure is taken to be: $p = \sin\theta R$. Per cent

$\overline{\sin\alpha}$ is judged to be about 0.3 from the pitch angle distributions published by Serlemitsos (1966). Thus, the partial pressures of energetic electrons in the cusp region vary from a small fraction of a percent to somewhat greater than one percent. If one assumes an energy spectrum reasonably steep down to 10 keV, then it appears that electrons $\geq$5 keV could supply a considerable fraction of the particle pressure necessary to support the observed, sharp magnetic field jump at the cusp boundary.

II. Broad Magnetic Depressions in the Geomagnetic Tail

We have discussed how the magnetic field usually undergoes a sharp jump through the particle cusp boundary. Beyond this boundary the field remains strong for distances of several earth radii. Field strengths of 30 to 40γ are attained. Figure 1 illustrates this strong field region extending from 15.1 R_e to about 22 R_e. In Fig. 2 the strong field is seen from 11.1 to about 16 R_e. A third example is given in Fig. 3 where a strong magnetic field is seen to extend from 13.5 R_e to 23.5 R_e. In all these cases the field becomes weaker at some larger geocentric distance. After remaining at a low value for distances of 5 or 10 R_e the field often recovers. In some cases such as the one in Fig. 3 the field is still weak (~3γ) at the satellite apogee. It presumably recovers at larger than 32 R_e in these cases.

Such depressions in the magnetic field magnitude several earth radii in extent are found on most orbits beyond the strong field region just discussed. These depressions sometimes contain an observed neutral sheet; at other times, although the depression is well developed, it does not contain an observed neutral sheet

crossing. However, in this latter case the Z_{sm} coordinate has become small showing that the measurements pertain to regions close to the theoretical position of the neutral sheet. Examples of this effect can be seen in most of the figures. In particular, Figs. 1, 2 and 4 are well developed examples. Although Ness (1965) has shown the field direction changes by approximately 180° in a small distance (~1000 km) during a neutral sheet crossing, the field is substantially weakened over much larger (~30,000 km) distances from the neutral sheet. Energetic electron fluxes are found to have a definite, although complex, association with these weak magnetic field regions deep in the tail of the magnetosphere. This association can be illustrated by orbit 34 inbound (Fig. 2). In this case, no neutral sheet crossing is observed but the satellite makes a very close approach to the solar-magnetospheric $Z_{sm} = 0$ coordinate plane. Furthermore, the field does briefly reverse direction three times while in this region at 23, 24 and 25 R_e. On this orbit the magnetic depression abruptly begins at a geocentric distance of 28 R_e and the directed distance from the $Z_{sm} = 0$ plane is -7.2 R_e. In the region 25 to 23 R_e the field becomes very weak taking on values as low as 2 or 3γ. In this region the Z_{sm} coordinate varies from -2 to 0 R_e. The inner boundary of this magnetic depression is rather difficult to locate precisely since it occurs in the strong field region just beyond the particle cusp at about 15 R_e. Across this entire region from 28 to 15 R_e there occur energetic electron fluxes, many of which show the characteristic fast-slow behavior of electron islands with flux peaks ranging from 1.5 to $6 \times 10^5 cm^{-2} sec^{-1}$.

They define an envelope which conforms very closely to the magnetic depression. This kind of field-particle association can be found on many of the orbits of IMP-1 in the geomagnetic tail and must be regarded as a basic feature of the geomagnetic tail region. A second example of this type of field-particle effect when the magnetic depression does not contain a neutral sheet crossing occurs on orbit 31 inbound and is shown in Fig. 1. The depression begins at 29 R_e where Z_{sm} is about -9 R_e and the field strength is 22γ. Between 25 and 27 R_e the field is weakest, sometimes dropping to 3γ. In this region the satellite comes within 3 R_e of the solar-magnetospheric equatorial plane. A smooth envelope which conforms closely to the magnetic depression may be drawn around the particle peaks. Other illustrations of this effect occur in Figures presented here. Figure 7 shows a good example from 24 to 14 R_e and Fig. 8 shows another from 31 to 22.5 R_e. Table IIa gives the location of all the large magnetic depressions without neutral sheet crossings found on the IMP-1 orbits in the geomagnetic tail. The flux of electrons >45 keV obtained at the maximum of the envelope containing the particle peaks is given in that Table. The Table also gives the Z_{sm} coordinate at the boundaries of the depression and at the location of the weakest magnetic field value. The ratio R is calculated as was done in Table I for the particle cusp-magnetic field association. In this case the particle flux used in the calculation is that which occurs at the maximum of the envelope constructed around the particle peaks. In all cases this is equal to or nearly equal to the highest peak flux over the region of magnetic depression. The value of F_{max} is usually obtained from the distant side of the depression. This procedure may be questioned on the basis

that stronger fields usually occur to the earthward side of the magnetic depression. These fields may be 10 to 20% stronger than the fields on the distant side of the depression. However, the fields in the region 12-15 R_e may still be magnetostatically supported to some degree by the dipole-like field and the diamagnetism of the cusp region may also partially account for this strong field. For these reasons we have chosen to obtain F_{max} at the larger geocentric distance.

Table II shows that the magnetic depression begins at large distances from the theoretical position of the neutral sheet. Lower limits to the actual distance from the neutral sheet can be obtained by subtracting the smallest Z_{sm} value attained on each orbit from the Z_{sm} value at the outer boundary of the depression. These lower limits range from 2 to 8.5 R_e below the magnetospheric equator. On the interpretation that the magnetic field depression is due to diamagnetic effects of charged particle populations these particles extend below (and presumably above) the neutral sheet for very large distances. The ratio R is calculated for each of the well-developed cases of magnetic depression without neutral sheet crossing. The value of this ratio varies from 0.05 to 1.7%. The larger values are usually accompanied by moderate or large daily Kp sums while the extreme low value occurs during and following an extremely quiet period.

We apply the same interpretation to the large magnetic depression that was done for the field particle association in the cusp: the magnetic field decrease is due to diamagnetic effects of charged particles. The R values given in Table II are based on the peak energetic electron flux occurring in the

magnetic depression. Most values fall in the range 0.5 to 1.7%. Between the peaks R becomes much less and energetic electrons play a much smaller role in providing the required diamagnetic effect. The pitch angle distribution of the energetic electrons when they appear is not known from the present measurements. However, some results from the Vela satellite measurements (Coon, 1965) suggest that these fluxes may be more or less isotropic. In that case $\overline{\sin\alpha} \approx 1$ and the partial pressures, $p = \sin\alpha\, R$, found from Table II lie mostly in the range 0.5 to 1.7%. It is interesting that these values are close to the values found in the particle cusp region. Thus the particle spectrums occurring in the tail at the time sporadic island fluxes of energetic electrons appear seem to have the same quality (hardness or softness) as the fluxes existing most of the time in the cusp region. This points to a connection between these two regions but this result does not decide the net direction of particle flow.

A simple average of R has been taken for the seven cases of magnetic depression without neutral sheet crossing. The value is 0.8%. This was also done in Table I for the field-cusp particle association. The value in that case was 2.5%. The Kp daily sum average is not much different in the two cases. As has been just discussed, due to a difference in pitch angle distribution the energetic electrons appearing in the tail may exert the same partial pressure as do particles of the same energy in the cusp region closer to the earth. On the other hand, between the energetic particle peaks in the tail region the magnetic depression still persists to about the same degree and the particle pressure

is then supplied by a particle spectrum of different form.

An example of a particle-field correlation in which a broad magnetic depression does contain a neutral sheet crossing occurs during orbit 38 inbound (Fig. 4). The depression begins at 25 R_e where Z_{sm} is -2 R_e, the neutral sheet crossing is at 20.1 R_e and the inner boundary of the depression is taken to be 15.1 R_e. Again an envelope may be constructed around the particle fluxes in this region which conforms well to the magnetic depression. On this orbit a broad magnetic depression without neutral sheet crossing is also present from 31 to 26 R_e. In this case the conformity of the particle envelope to the magnetic depression is not as good as in the three examples discussed above. The depression is again associated with a close approach of the satellite to the $Z_{sm} = 0$ plane with values of Z_{sm} ranging from -5 to -1 R_e.

Another example is shown in Fig. 3. Here a series of small peaks of nearly uniform size defines an envelope which conforms to the magnetic depression surrounding the neutral sheet crossing.

Further examples of this type of field-particle correlation are shown in Figs. 5 and 9.

Table III gives information about the boundaries, Z_{sm} coordinates, magnetic field strengths and particle fluxes for all large magnetic depressions containing one or more neutral sheet crossings on the IMP-1 orbits. The ratio in Table III is calculated in just the same manner as it was in Table II. The same criteria for assigning particle fluxes, F_{max} and F_{min} values were used so these two tables are directly comparable.

The R values now range from 0.06 up to 0.9%. The average for the seven cases is 0.28%. This is a factor of three smaller than the average in Table II. The average daily Kp sum is the same in both tables so this is not an effect of geomagnetic activity. The conclusion is then that when the satellite moves close to and through the neutral sheet it encounters particle populations in which energetic electrons play only a small role in exerting the required pressure against the magnetic field. We have argued that the broad magnetic depressions without neutral sheet crossing differ only in that the trajectory of the satellite did not quite cut the neutral sheet. Therefore, the region immediately surrounding the neutral sheet to $\gtrsim 1$ R_e evidently contains an appreciably softer population of particles than do the regions still within the same magnetic depression but beyond 1 R_e from the neutral sheet.

The broad magnetic depressions in the geomagnetic tail discussed here are most likely a manifestation of the plasma sheet required to prevent the tail from collapsing at the neutral sheet, where the field reverses. This interpretation is based on two main points: First, the magnetic depressions show systematic behavior when described in terms of distance from the solar-magnetospheric equator, and second, the extent of the magnetic depressions along this plane are at least 10 to 15 R_e. The IMP-1 satellite gives this value as a lower limit since it remains close to the solar-magnetospheric equator only for these distances.

Recently, the Vela group (Bame, et al, 1966) has measured

electron fluxes over the energy range 0.35 to 20 keV at a geocentric distance of 16-18 R_e in the geomagnetic tail. They found electron kinetic energy densities of 0.26 to 1.0 x 10^{-9} $\frac{ergs}{cm^3}$ on one particular orbit. The magnetic field was not measured simultaneously on this satellite so it is not possible to directly test this energy density to see if it is sufficient to account for the magnetic depressions discussed here. For the single case reported, the electron energy density if doubled to take into account the proton contribution, could reduce a 16 gamma field to 5 or 10 gammas. The IMP-1 measurements of magnetic field at 17 R_e show that out of 17 passes through this region the magnetic field was as low as 16 gammas on 8 occasions. Thus, there is a good probability that the Vela electron detectors were seeing fluxes sufficiently high to account for the diamagnetic effects observed by IMP-1 in the tail.

There is a feature of the energetic electron fluxes associated with the large magnetic depressions in the tail that deserves further discussion. This is the marked tendency for the flux peaks to form a smooth envelope. Again turning to the examples in Fig. 1, it is seen that the largest flux peaks occur near the center of the broad magnetic depression that extends from 29.5 R_e to about 19 R_e. Toward the boundaries of this depression the flux peaks and the associated envelope fall off by a factor of 5. Figure 2 gives an example where the 10 or 12 largest flux peaks are uniform within a factor of 2 or 3 over the magnetic depression that extends from 28 to 15 R_e. Again in Fig. 3 examples of the coherence in intensity of the flux peaks

can be seen. The same effect can be seen in fact in most of the figures given here. One of particular interest occurs on orbit 39 in Fig. 9. Here the flux peaks are strikingly uniform over a distance of ~13 R_e and times of ~20 hours.

The conformity of the particle envelope to the magnetic depression implies that the energetic particles are closely related to the low energy particles producing the bulk of the diamagnetic effect. It would appear, therefore, that some physical process occurs over these very large regions in a way such as to raise some particles to higher energies over this entire region for some minutes or hours. Recent Vela satellite measurements (Bame, et al, 1966) clearly show that in the tail a rapid change in the spectral form of the entire electron population takes place with a small fraction of the electrons attaining energies above 45 keV.

The cause of this energization is not known but the suddenness with which it takes place suggests an instability which releases energy, a hydromagnetic shock, or a sudden injection from another region of the radiation zone.

In this section much but not all of the field and energetic electron data from the IMP-1 satellite has been presented to illustrate the three field-particle correlations just discussed. Data is available from seventeen IMP-1 satellite orbits which occur fully within the geomagnetic tail. The data discussed here is obtained from the inbound portion of these orbits. The outbound portions are not used because: (a) the satellite does not go into the cusp region during outbound passes since these are always

at high southerly magnetic latitudes and (b) because the broad magnetic depressions are rarely observed due to the large Z_{sm} values reached by the satellite on the outbound portions of the orbits.

In order to illustrate further the fact that the effects discussed here are a persistent feature of the field and particle behavior in the geomagnetic tail we present the inbound portions of all the remaining tail orbits. These will also serve to illustrate those occasions when field-particle correlations are not well developed. An additional reason for presenting all orbits is that full publication of these results will enable those who wish to do so to make correlation studies with data from other satellite experiments, with balloon experiments and with ground-based apparatus. The remaining inbound tail orbits are given in Figs. 13-18. Some discussion will be presented here concerning each of these figures. Figure 13 illustrates all three of the field-particle correlations discussed above. The inflated magnetic field in the cusp is pronounced and several instances of a close field-particle association occurs for electron island fluxes. In this case the magnitude of the tail field fluctuates greatly during the orbit. This may partially account for the fact that the broad magnetic depressions in the tail, while present are not as well developed as in some of the previous examples. A geomagnetic storm was in progress during this orbit. Figure 14 illustrates quite well the inflated magnetic field in the particle cusp. The cusp boundary is taken to occur at 15.5 R_e but it is not clear whether the boundary is there or at 11.2 R_e. Figure 15 shows a situation where the magnetic field is being depressed by particles in the cusp region.

However, the magnetic field does not show a well defined jump where the particle fluxes do. Figure 15 also shows a very weak field beyond 27 R_e but only very weak electron fluxes above 45 keV. Evidently this depression of the geomagnetic field is being produced by particles of lower energy. The inflation of the magnetic field in the particle cusp during orbits 33 and 32 (Figs. 16 and 17) is not apparent although substantial fluxes are present. However, in these cases the reversal of field direction is occurring much closer to the earth than is the case for the other orbits. A magnetic storm was in progress during orbit 33. The geomagnetic indices were very low during orbit 32. Figure 18 shows two broad depressions in the tail field associated with moderate (5×10^4 $cm^{-2}sec^{-1}$) electron fluxes. A neutral sheet crossing occurs in one of these depressions.

III. Correlation of Individual Electron Island Fluxes with Magnetic Field Features.

The preceding analysis has made it clear that energetic electron fluxes in the geomagnetic tail are associated with large magnetic depressions which have radial extent on the order of 10 R_e. The particles and associated magnetic depression reach far beyond the observed positions of the neutral sheet and far beyond the solar-magnetospheric $Z_{sm} = 0$ plane. Electrons >45 keV may appear as far away as $Z_{sm} = -9$ R_e and usually show no strong tendency to appear preferentially at the neutral sheet. However, energetic particle fluxes often do occur there and it is of interest to further investigate their distribution with respect to the neutral sheet.

It is again useful to refer to several examples to show the wide range of peak flux values and of flux profiles encountered in and near the neutral sheet as defined by the magnetometer. First of all, crossings of the neutral sheet clearly within the particle cusp region will not be considered here. As Serlemitsos (1966) has shown, the field lines in this region are closed (although the radial distance of the boundary of this region may be quite time dependent). The neutral sheet data in this region reflects the fact that the component of the field line projected on a coordinate plane undergoes a sudden reversal although the field line itself changes only by a small amount.

Figures 4 and 8 are examples of energetic electron fluxes extending over a radial distance of several earth radii more or less centered on a neutral sheet crossing. In the eleven IMP-1 orbits within the geomagnetic tail which contain fifteen observed neutral sheet crossings, there is only one other example of particle fluxes which arrange themselves in such symmetrical fashion.

There does seem to be a tendency for the peak energetic electron fluxes associated with neutral sheet crossings to occur some distance on the earthward side of the crossings. Due to the mixing of spatial coordinates imposed by the satellite's trajectory this effect might be associated with other parameters. Another spatial coordinate which changes rapidly is Z_{SM} so that the fluxes have a tendency to occur somewhat away from the neutral sheet at positive values of Z_{SM} of a few earth radii. Examples of this tendency for particles to occur off the neutral sheet occur on five of the tail orbits. Three of these cases are given here in Figs. 5, 9 and 10. Figure 11 (orbit 40) also shows this effect.

In three cases, no particle fluxes or only very weak fluxes were present in or near the observed neutral sheet. In one case the flux was detectable and was about 5000 $cm^{-2}sec^{-1}$, but this is much smaller than the fluxes observed throughout most of the inbound portion of that particular orbit. The occasional paucity of energetic particles at the neutral sheet is illustrated by Fig. 5 for the first of the two crossings made by the satellite and in Fig. 6.

The distribution of electron island fluxes in solar ecliptic, geomagnetic and solar magnetospheric coordinates is shown in Fig. 12. Each of the 120 electron islands observed on the tail orbits are plotted against the Z coordinate in the three coordinate systems. The results of this are the curves marked actual. Not all values of Z_{sm} are encountered by the satellite with the same frequency over the 17 tail orbits. The relative frequency of the satellite's position taking on a given Z value is plotted against that Z value. This curve is based on the actual trajectories of the satellite for orbits 31 through 47. The result is the curve marked predicted. The degree to which the two curves are similar represents the degree to which the particular coordinate system organizes the data. The implicit assumption is that the frequency of occurrence of islands is the same at all geocentric distances. This is true to no better than a factor of two so a very close agreement between the pairs of curves cannot be expected.

In the solar ecliptic coordinate system there appears to be a deficiency in the number of islands when the satellite is

located below the ecliptic plane. Therefore, during the interval 15 March to 3 June 1964 the satellite data show a preference for island occurrences above the ecliptic plane.

For the geomagnetic coordinate there is a tendency for the islands to occur less frequently at large southerly magnetic latitudes, between 8 to 16 degrees, while this observed distribution indicates an enhanced occurrence for magnetic latitudes between -5° and $+3^{\circ}$. The coverage in geomagnetic latitude is limited and it is not easy to determine if the geomagnetic equatorial plane is a preferred plane of orientation for island occurrences.

The lower curve of Figure 12 compares the occurrences with that predicted in the solar magnetospheric coordinate system. Here it is seen that the satellite positions are broadly distributed about the solar magnetospheric equatorial plane. For latitudes which correspond to positions of the satellite more than $\pm 5\ R_e$ from the solar magnetospheric equatorial plane the number of island occurrences is less than to be expected. For positions of the satellite within $\pm\ 5\ R_e$ of the solar magnetospheric equatorial plane the occurrences are slightly higher than expected. However, there are no gross departures between the actual and predicted curves, and they give evidence that island fluxes are distributed symmetrically with respect to the solar-magnetospheric equator. The three distributions are consistent with a distribution which near the earth is dominated by the geomagnetic equatorial plane but such that at greater distances into the tail the solar magnetospheric coordinate system becomes more appropriate.

The largest electron fluxes observed in the tail region often are associated in a detailed way with magnetic field decreases. Orbit 40 shown in Fig. 11 is the best example of this. There, excellent agreement of the electron flux and magnetic field profile are to be seen. R values for these associated field-particle changes are about 1.5% although the choice of F_{max} values are somewhat arbitrary in this case. It is particularly difficult to arrive at an R value for the neutral sheet crossing at 20 R_e and the R value there could be either 0.3% or 1% depending on the choice of F_{max}. The Kp indices were low at the time of satellite measurements but a geomagnetic storm had occurred during the previous three days.

Most orbits do not show such good particle peak to magnetic valley correlations as does orbit 40. However, other examples may be found in the figures here: Fig. 6, 19 to 17.5 R_e and Fig. 7, 17.8 to 16 R_e. The R value for the first of these two peaks is 3.4%.

SUMMARY

Three types of diamagnetic effects of charged particle populations have been identified on the dark side of the Earth. In the particle cusp region it appears that energetic electrons may account for much of the observed diamagnetic effect. Where the geomagnetic tail has become fully developed, broad depressions of the magnetic field extend northward and southward from the neutral sheet by ~5 R_e in each direction. These regions are from a few up to 15 R_e in radial extent. They may in fact extend along the neutral sheet for much larger distances and probably are to be identified with the plasma sheet providing the required particle pressure to prevent collapse of the tail field into the neutral sheet. Particle fluxes occur throughout these regions and show a coherence in the sense that the peak fluxes are not random but are related to neighboring peaks.

Energetic electron fluxes do not show a strong preference to occur in the neutral sheet. The peak fluxes in and around neutral sheet crossings do not exceed those observed elsewhere on the same orbit. There is some evidence that the energetic particles in fact avoid a small region (≈1 R_e) in and around the neutral sheet. This may in part be due to the fact that a charged particle with guiding center on a magnetic neutral surface undergoes only part of a gyration about the lines before the radius of curvature reverses. Thus the particle can readily move "across" lines of force and out of the neutral region.

It is of interest to attempt a self-consistent model for the observed behavior of the magnetic field and the energetic particle fluxes in the geomagnetic tail. In particular, their inter-

relationships in the large depressions surrounding the neutral sheet will be of most interest because of the transient character of both the magnetic field and particle flux features.

Since they have been observed on all the IMP-1 orbits in the geomagnetic tail it is assumed that the broad depressions are a permanent feature of the geomagnetic tail. Their close spatial relationship to the neutral sheet suggests further that they are a consequence of the neutral sheet. Permanent populations of particles, sometimes containing electrons >45 keV, are responsible through their diamagnetic effects for weakening the field in this region. It is noticed that the field magnitude in the central part of the depressions does not vary greatly. It usually remains between 5 and 8γ. The field surrounding it varies over the range 10γ to 40γ. We suppose the increase in the tail field to be an effect of the solar wind during disturbed times, (Behannon and Ness, 1966). The failure of the field to increase appreciably inside the magnetic depression is attributed to the fact that any attempt to increase the field is partially compensated by increased particle energies which in turn produce an enhanced diamagnetic effect. The appearance of electron island fluxes showing characteristic fast-slow behavior may be due to the presence of propagating hydromagnetic shock waves. Conditions favor shock formation when the field is strong (~30γ) on the outside of the magnetic depressions in which the field is typically 5 to 8γ. At these times a disturbance such as a train of hydromagnetic waves moving through the strong field region and arriving at a weak field may steepen into a shock.

The hypothesized source of disturbance in the outer, strong-field region is the solar wind. There is strong evidence to support frequent hydromagnetic wave activity throughout the tail region (Lin and Anderson, 1966). There is also evidence that these hydromagnetic disturbances couple strongly to electrons and alter their energy by some tens of kilovolts. Thus as the shock waves move into the region of magnetic depression they elevate the energy of electrons resulting in the observed island fluxes.

For a hydromagnetic disturbance propagating in a region where the ambient field is 5γ, the energy density in the wave cannot exceed about 10^{-10} ergs/cm^3. By comparison a flux of electrons >45 keV of 10^6 cm^{-2}sec^{-1} has an energy density of 0.4×10^{-10} ergs/cm^3. The wave therefore appears to carry sufficient energy to accelerate particles in the observed way but the efficiency of coupling would have to be high.

The accelerated particles often have a strong diamagnetic effect as can be seen in Fig. 11. It may be sufficient to form a local magnetic bottle in which the particles remain, slowly leaking out, until finally the bottle becomes unstable and the particles suddenly disappear.

TABLE I

Orbit Number	Geocentric Distance of Particle Cusp Boundary	Change in Energetic Electron Flux Across Cusp Boundary	$\overline{F}_{max}$ Averaged Field Magnitude Outside Cusp	$\overline{F}_{min}$ Averaged Field Magnitude Inside Cusp	R	Kp Sum
31	15.2 R_e	1 x 10^7 $cm^{-2}sec^{-1}$	29γ	14γ	4.5%	24
34	11.0	1 x 10^7	40	30	4.1	19
37	11.1	2 x 10^7	45	25	4.1	24
38	14.9	2 x 10^6	26	15	1.3	4
40	9.9	1 x 10^6				
41	9.9	5 x 10^6				
44	13.4	2 x 10^6	27	9	1	29
45	11.8	2 x 10^6	25	13	1.3	10
46	13.6	3 x 10^5	29	11	0.12	11
47	12.2	1 x 10^7	36	21	3.2	20
					Average 2.5%	18

TABLE II

Orbit Number	Outer Boundary of Magnetic Depression		Bottom of Magnetic Depression		Peak Flux Electrons >45 keV in Depression	$\overline{F}_{max}$	$\overline{F}_{min}$	R	Kp Sum
	Geocentric Distance	Z_{sm}	Geocentric Distance	Z_{sm}					
31	29.5 R_e	-9.4 R_e	25.5 R_e	-3 R_e	$1 \times 10^6 cm^{-2} sec^{-1}$	23γ	5γ	0.6%	25
32	28.5	-6.5	27.5	-3	3.5×10^3	10	3	0.05	1,7
33	29.3	-9.5	25 ± 1	-1	6×10^6	34	9	1.4	30
34	28	-7	23	0	7×10^5	21	4	0.5	12
35	24.3	-2	20	0	2.1×10^6	19	5	1.7	9
36	23	-1.2	19	+1.4	6.3×10^5	21	5	0.43	8
41	>32	-	28	0	1×10^6	19	3	0.9	18
							Average	0.8%	15

TABLE III

Orbit Number	Outer Boundary of Magnetic Depression		Bottom of Magnetic Depression		Peak Flux Electrons >45 keV In Depression	$\overline{F}_{max}$	$\overline{F}_{min}$	R	Kp Sum
	Geocentric Distance	Z_{sm}	Geocentric Distance	Z_{sm}					
37	>32 R_e	-	23 R_e at N.S.	-1.8 R_e	2.8×10^5 $cm^{-2}sec^{-1}$	35γ	13γ	0.09%	24
38	25	-2	20.1 at N.S.	0	1.7×10^5	20	5	0.14	16
39	24	-1	19.6 at N.S.	+0.3	1.4×10^6	27	8	0.6	19
42	18.5	+2.8	15.3 at N.S.	+2	7×10^4	23	16	0.07	5
43	31	+1	26 ± 2 two N.S. crossings	+2±0.5	2.1×10^6	30	5	0.06	25,20
45	24	+3.6	17.9 at N.S.	+3.9	8.4×10^5	20	9	0.9	9
46	>32	-	28.2	+2.8	2.8×10^5	30	4	0.09	7
							Average	0.28%	15

TABLE CAPTIONS

Table I - This table gives the magnetic field magnitude inside and outside the particle cusp boundary. The associated particle fluxes are also given and the quantity R is calculated. It can be seen that there is some tendency for large R values to be accompanied by large Kp daily sums. This implies some degree of hardening of the fluxes in the cusp region during geomagnetic activity.

Table II - This table gives field magnitudes and particle fluxes inside and outside broad magnetic depressions in the geomagnetic tail that do not contain neutral sheet crossings. The R values average to about 3% and again these values are organized somewhat by the Kp daily sums.

Table III - In the broad magnetic depressions that contain a neutral sheet crossing the R value is very low indicating a very soft particle population with ~1 R_e of the neutral sheet.

FIGURE CAPTIONS

Figure 1 - The particle cusp region on this orbit is associated with a decreased magnetic field beginning at 15 R_e, coincident with the particle boundary, and extending in at least as far at 10 R_e. Inside this distance the magnetic field rapidly becomes stronger, approximately as R^{-3}. The weakened field region inside 15 R_e shows much variability. Beyond 15 R_e the field becomes quite strong and remains so until about 22 R_e where it weakens greatly. This depression of the magnetic field extends to nearly 30 R_e and is associated with a close approach to the Z_{sm} coordinate plane. Energetic electron fluxes occur throughout this weak field region but the field remains weak even when these fluxes occasionally disappear.

Figure 2 - The outer boundary of the particle cusp region coincides with a magnetic field weakening at 11.2 R_e. The field drops from about 41γ to 28γ. Also on this orbit a broad magnetic depression is seen from 28 R_e in to about 16 R_e where the field becomes quite strong. Again most of the particle fluxes appear in the broad weak field region from 16 R_e to 28 R_e.

Figure 3 - The magnetic field in the cusp region is greatly weakened by charged particles. The particle flux and the magnetic fields jump simultaneously at 13.5 R_e. Beyond this the field is strong to 24 R_e where it suddenly weakens due to the approach within 2 earth radii of the neutral sheet. The neutral sheet is seen to occur at 2.5 R_e. Groups of energetic electron peaks again appear confined mainly to the depressed magnetic field region.

Figure 4 - Two apparently distinct broad magnetic field regions occur on this orbit. Each has a group of energetic electron fluxes with coherent peak fluxes. The diamagnetic effect of the particles in the cusp region is well illustrated in this figure.

Figure 5 - A magnetic depression extends across the first neutral sheet crossing at ~7 R_e. This depression is about 4 R_e in radial extent and ~.5 R_e in the Z_{SM} coordinate. In this case only very weak (~3000 $cm^{-2}sec^{-1}$) energetic electron fluxes are present. A much broader depression containing a neutral sheet crossing appears from ~3.8 R_e in to about 1~ R_e. Again, the fluxes near the neutral sheet are not larger than other fluxes in this region. The field weakening in the particle cusp is again well defined.

Figure 6 - Only very weak fluxes of electrons >45 keV appear at the neutral sheet while much larger fluxes appear elsewhere on the orbit. The cusp effect is again well developed.

Figure 7 - In this case it is not possible to identify the cusp region due to absence of a well-defined particle jump. There are particles present in the region normally occupied by the cusp particles and there does appear to be some weakening of the magnetic field. A broad magnetic depression occurs from about 14 R_e to ~4 R_e and again most of the particle flux observed in the tail is within this region.

Figure 8 - A broad field depression occurs from >32 R_e to about 22 R_e and contains many particle peaks. The fluxes near the neutral sheet have an unusual appearance. The largest peaks are somewhat removed from the neutral sheet crossing.

Figure 9 - A series of particle fluxes of very nearly the same value extends over a magnetic depression for a distance of nearly 14 R_e. The island flux which occurs nearest the neutral sheet is no larger than other fluxes in this region. Within this island the peak flux value is reached more than an earth radius earthward of the observed neutral sheet crossing.

Figure 10 - For each neutral sheet crossing there is a moderately large flux of energetic electrons. In both cases the peak fluxes are earthward of the neutral sheet and to the north of it.

Figure 11 - On this orbit especially well developed detailed correlations between electron island fluxes and magnetic field decreases can be found. The rapid transient behavior of the three field quantities suggest shock wave activity. These in turn may couple to the particles resulting in acceleration.

Figure 12 - Distributions of electron island fluxes in the geomagnetic tail with respect to three coordinate planes. These are the solar ecliptic (SE), geomagnetic equatorial plane (MLAT) and the solar magnetospheric (SM).

Figure 13 - A well defined magnetic field jump of about 15γ occurs at the particle cusp boundary at 13.5 R_e. Geomagnetic activity is high resulting in many intense particle fluxes in the tail and, in those regions where particles are absent, strong magnetic fields.

Figure 14 - The cusp boundary is probably at 11.5 R_e on this occasion. However, an electron island flux occurs just beyond and appears related to the cusp. A broad depression of the tail field is evident between 19 and 28 R_e. Few energetic electrons occur in this depression, however.

Figure 15 - The cusp situation on this occasion is similar to the one shown in Fig. 14. Again an island flux appears to be related to the cusp.

Figure 16 - Energetic electrons are present out to 28 R_e during a geomagnetically disturbed period. These particles are associated with a broad magnetic depression. Beyond this the field is strong. The cusp region is difficult to identify.

Figure 17 - During a geomagnetically quiet period few energetic electrons are found in the tail and the tail field is also weak.

Figure 18 - In this example weak fluxes of energetic electrons are present several earth radii on either side of the neutral sheet.

REFERENCES

Anderson, K. A., Energetic electron fluxes in the tail of the geomagnetic field, J. Geophys. Res., 70, 4741-4763, 1965

Anderson, K. A., H. K. Harris and R. J. Paoli, Energetic electron fluxes in and beyond the earth's outer magnetosphere, J. Geophys. Res., 70, 1039-1050, 1965

Bame, S. J., J. R. Ashbridge, H. E. Felthauser, R. A. Olson and I. B. Strong, Electrons in the plasma sheet of the earth's magnetic tail, Phys. Rev. Letters, 16, 138, 1966

Behannon, K. W. and N. F. Ness, Magnetic Storms in the earth's magnetic tail, To be published, J. Geophys. Res., 71, 1966

Cahill, L. J., Jr., Inflation of the magnetosphere near 8 earth radii in the dark hemisphere, presented at COSPAR 1965, Buenos Aires, To be published, 1966, [illegible]del Publishing Co.

Coon, J. H., Vela satellite measurements of particles in the solar wind and the distant geomagnetosphere, Bergen Study Institute, 1965

Frank, L. A., A survey of electrons beyond 5 R_e with Explorer XIV, J. Geophys. Res., 70, 1593-1626, 1965

Freeman, J. W., Electron distribution in the outer radiation zone, J. Geophys. Res., 69, 1691-1724, 1964

Gringauz, K. I., V. G. Kurt, V. I. Moroz, and I. S. Shklovsky, Results of observations of charged particles observed out to 1000,000 km with the aid of charged particle traps on Soviet space probes, Astron. Zh., 37-4, 716-735, 1960

Lin, R. P. and K. A. Anderson, Periodic modulations of the energetic electron fluxes in the distant radiation zone, to be published, J. Geophys. Res., 71, 1966

Ness, N. F., The earth's magnetic tail, J. Geophys. Res., 70, 2989-3005, 196

Ness, N. F., C. S. Scearce and J. B. Seek, Initial results of the IMP-1 magnetic field experiment, J. Geophys. Res., 69, 3531-3570, 1964

Serlemitsos, P., Low energy electrons in the magnetosphere, J. Geophys. Res., 71, 61, 1966

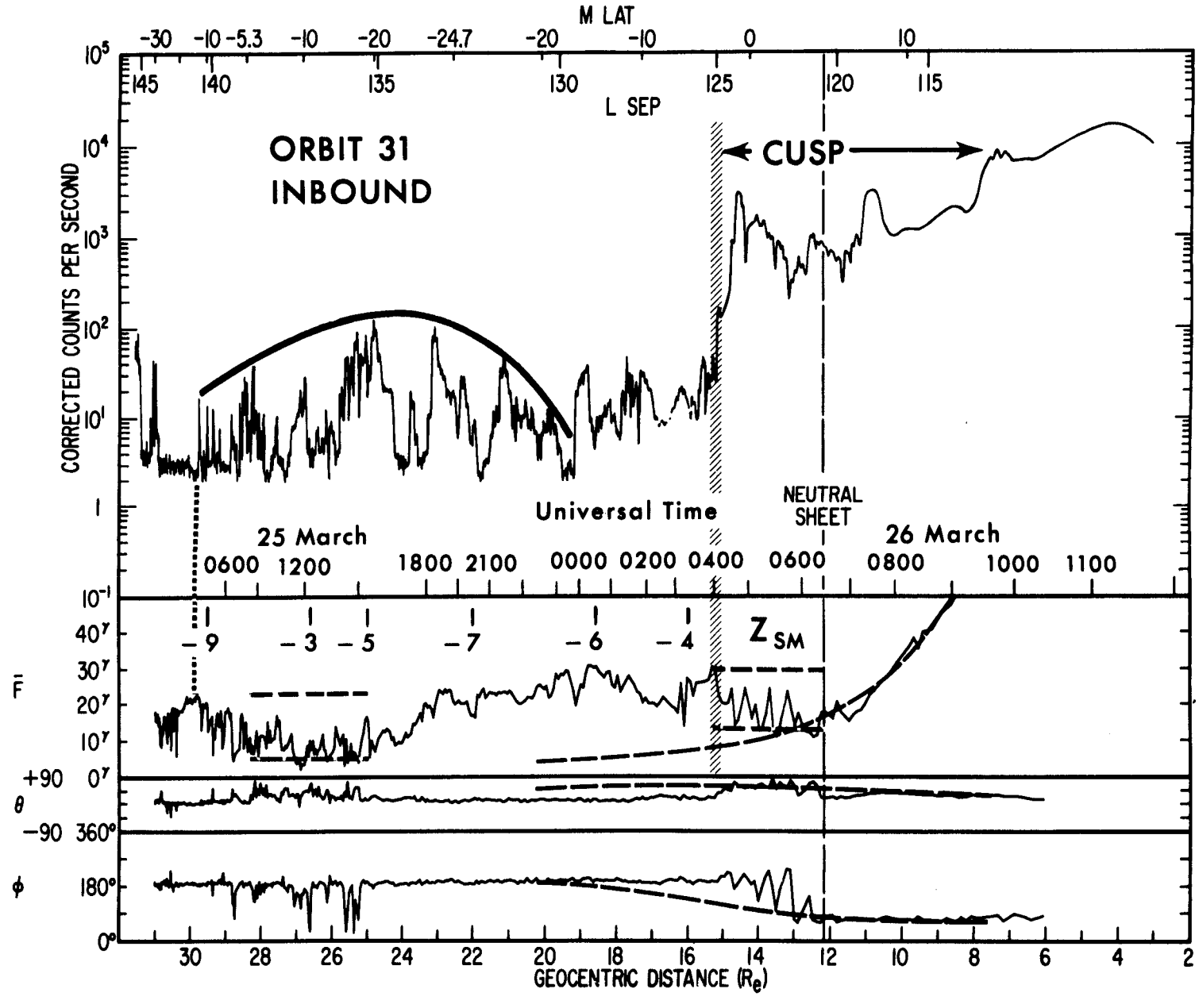
M LAT
-30 -10 -5.3 -10 -20 -24.7 -20 -10 0 10
145 140 135 130 125 120 115
L SEP
ORBIT 31
INBOUND
CUSP
CORRECTED COUNTS PER SECOND
Universal Time
NEUTRAL SHEET
25 March
26 March
0600 1200 1800 2100 0000 0200 0400 0600 0800 1000 1100
-9 -3 -5 -7 -6 -4
Z SM
F
θ
φ
GEOCENTRIC DISTANCE (Re)

Figure 1

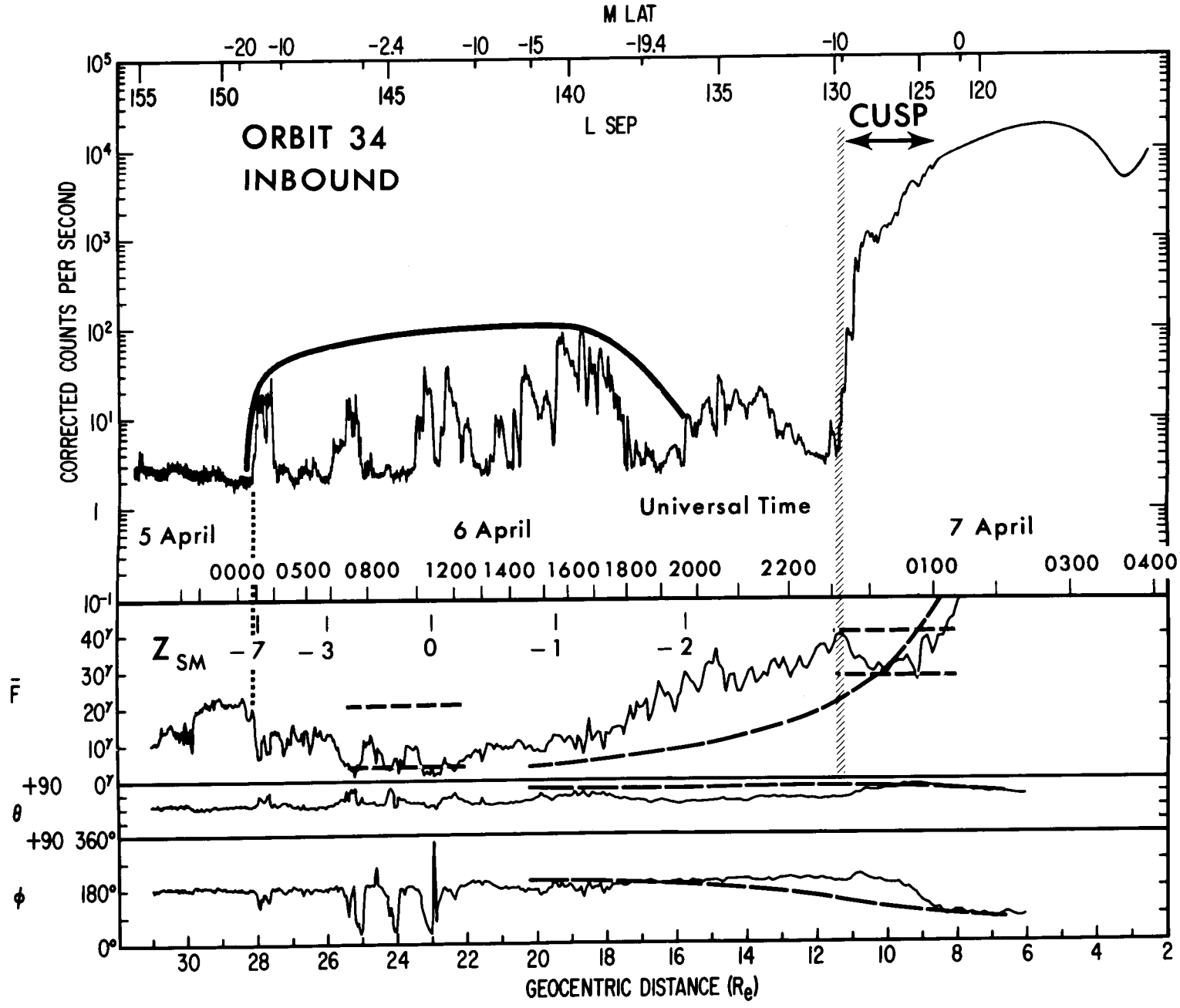
M LAT
-20 -10 -2.4 -10 -15 -19.4 -10 0
155 150 145 140 135 130 125 120
L SEP
ORBIT 34
INBOUND
CUSP
CORRECTED COUNTS PER SECOND
Universal Time
5 April
6 April
7 April
0000 0500 0800 1200 1400 1600 1800 2000 2200 0100 0300 0400
Z SM
-7 -3 0 -1 -2
F
θ
φ
GEOCENTRIC DISTANCE (Re)

Figure 2

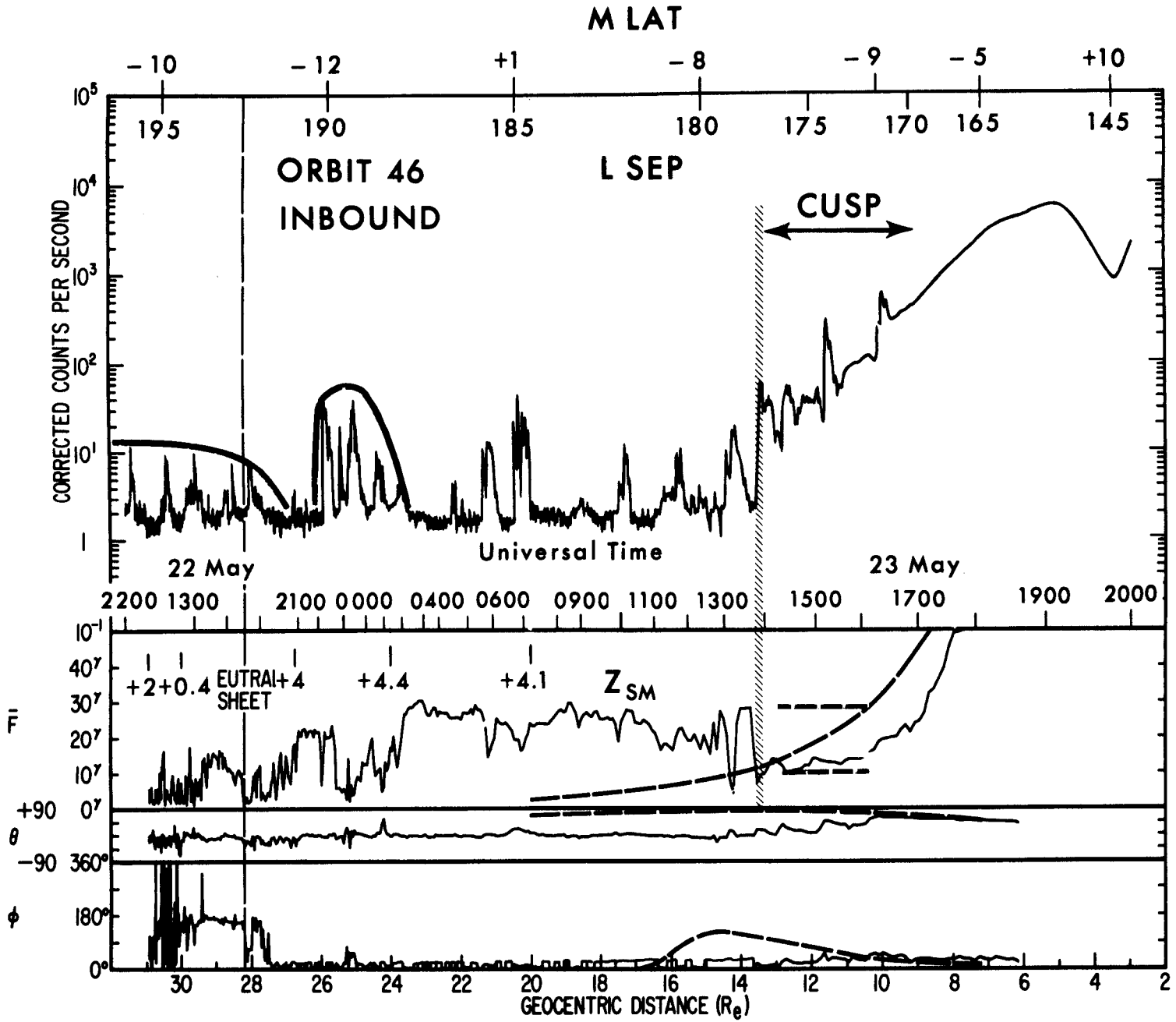
M LAT
-10
-12
+1
-8
-9
-5
+10
195
190
185
180
175
170
165
145
ORBIT 46
INBOUND
L SEP
CUSP
CORRECTED COUNTS PER SECOND
Universal Time
22 May
23 May
2200 1300
2100 0000 0400 0600 0900 1100 1300
1500 1700 1900 2000
+2+0.4
EUTRAI+4
SHEET
+4.4
+4.1
Z_{SM}
F
θ
φ
GEOCENTRIC DISTANCE (R_e)

Figure 3

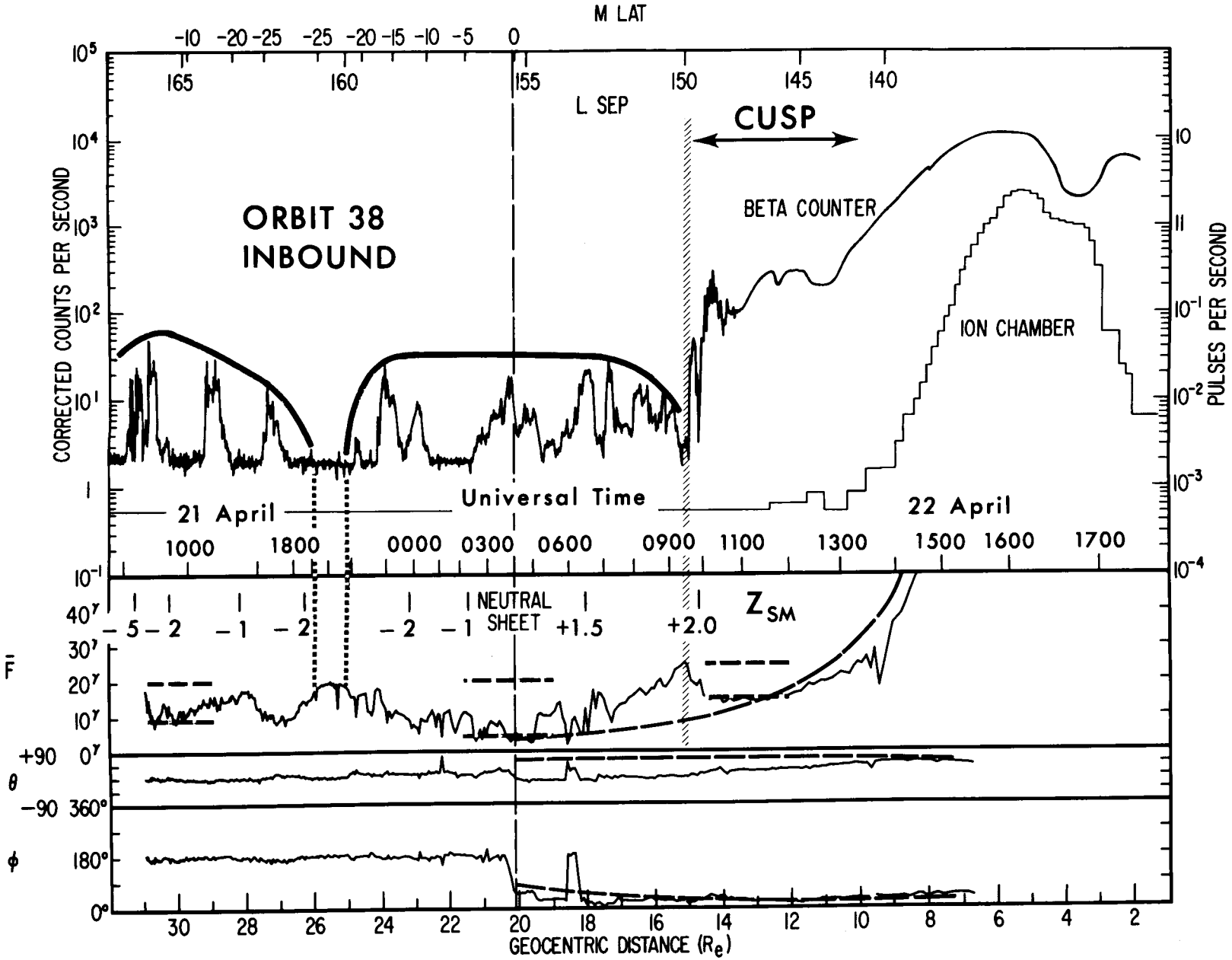
M LAT
-10 -20 -25 -25 -20 -15 -10 -5 0
165 160 155 150 145 140
L SEP
CUSP
ORBIT 38
INBOUND
BETA COUNTER
ION CHAMBER
CORRECTED COUNTS PER SECOND
PULSES PER SECOND
21 April
Universal Time
22 April
1000 1800 0000 0300 0600 0900 1100 1300 1500 1600 1700
NEUTRAL SHEET
-5 -2 -1 -2 -2 -1 +1.5 +2.0
Z_{SM}
F
θ
φ
+90
-90
360°
180°
0°
GEOCENTRIC DISTANCE (R_e)

Figure 4

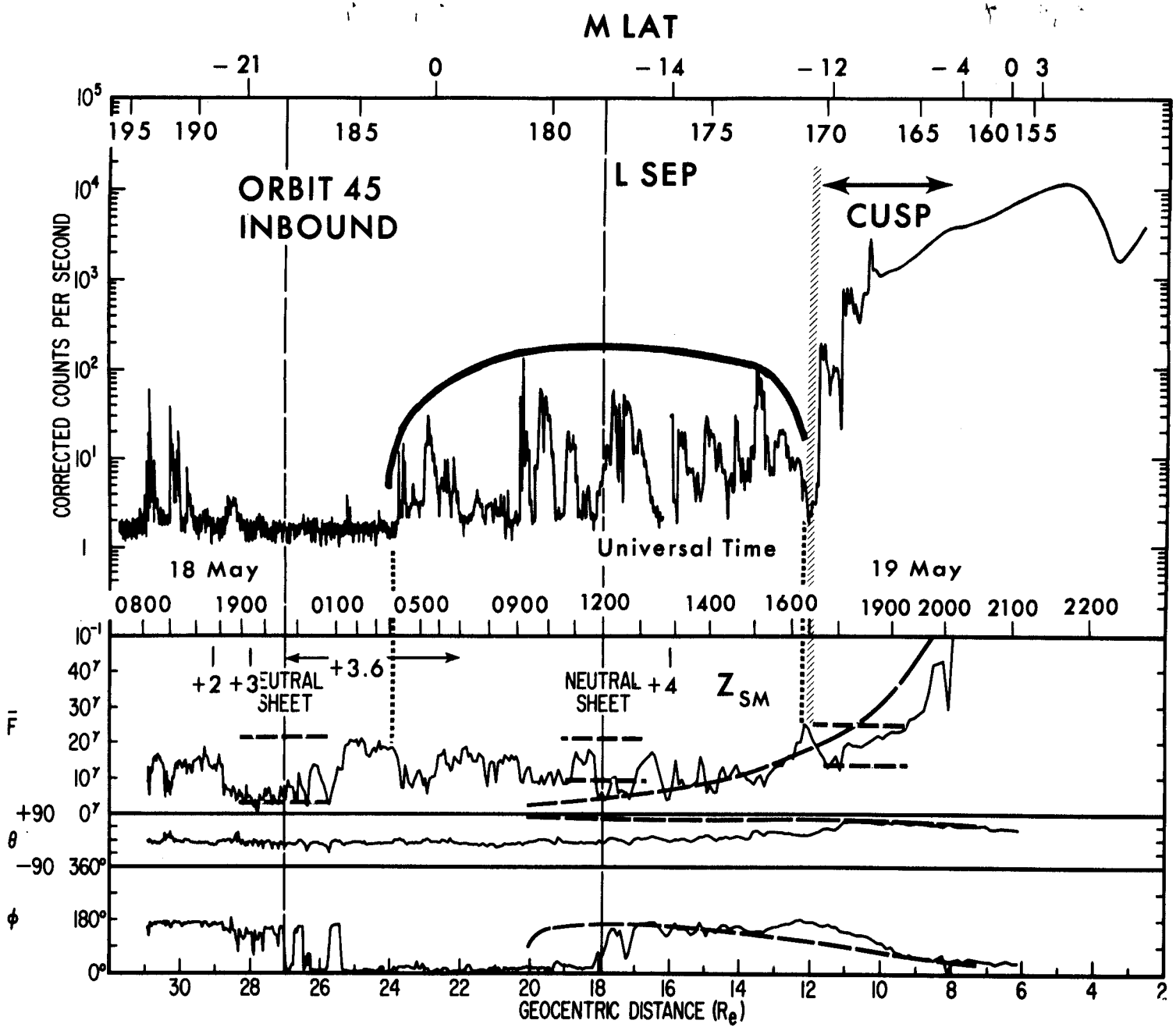
M LAT
-21
0
-14
-12
-4
0
3
195
190
185
180
175
170
165
160
155
ORBIT 45
INBOUND
L SEP
CUSP
CORRECTED COUNTS PER SECOND
Universal Time
18 May
19 May
0800
1900
0100
0500
0900
1200
1400
1600
1900
2000
2100
2200
+2
+3
NEUTRAL SHEET
+3.6
NEUTRAL SHEET
+4
Z_{SM}
F
θ
φ
+90
-90
360°
180°
0°
GEOCENTRIC DISTANCE (R_e)

Figure 5

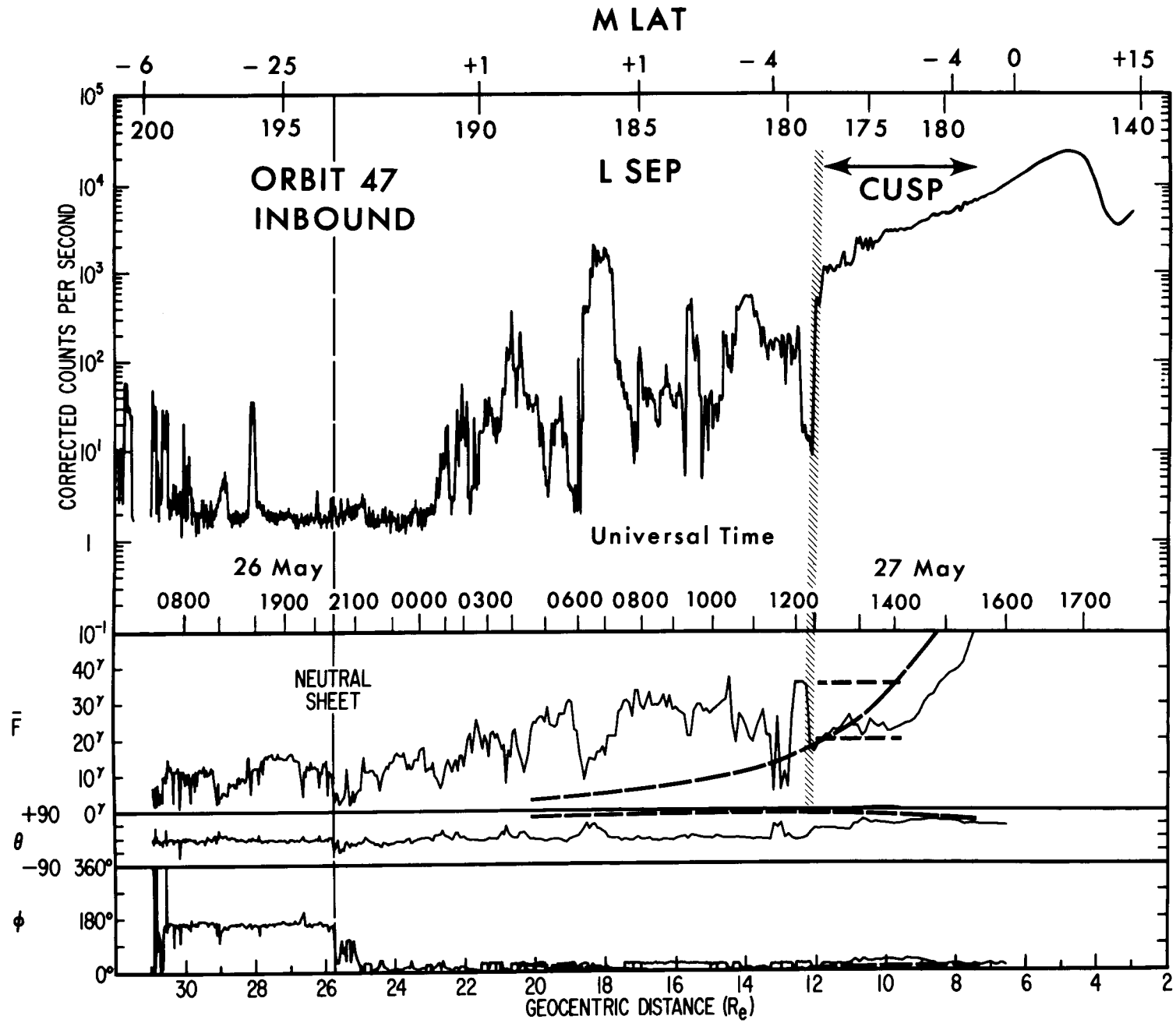
M LAT
- 6
- 25
+1
+1
- 4
- 4
0
+15
200
195
190
185
180
175
180
140
L SEP
ORBIT 47
INBOUND
CUSP
CORRECTED COUNTS PER SECOND
Universal Time
26 May
27 May
0800
1900
2100
0000
0300
0600
0800
1000
1200
1400
1600
1700
NEUTRAL
SHEET
F
θ
φ
+90
-90
360°
180°
0°
GEOCENTRIC DISTANCE (Re)

Figure 6

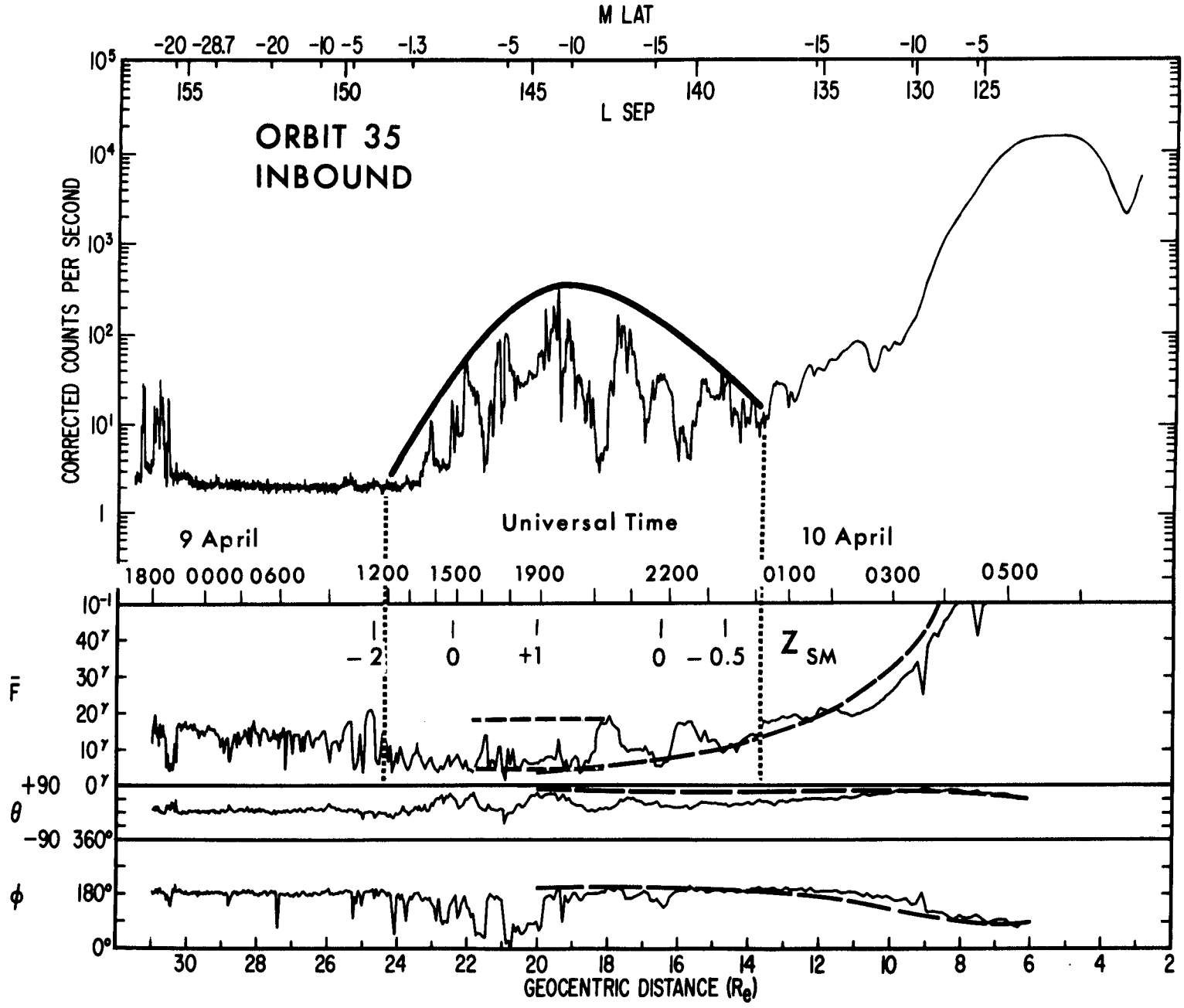
M LAT
-20 -28.7 -20 -10 -5 -1.3 -5 -10 -15 -15 -10 -5
155 150 145 140 135 130 125
L SEP
ORBIT 35
INBOUND
CORRECTED COUNTS PER SECOND
Universal Time
9 April
10 April
1800 0000 0600 1200 1500 1900 2200 0100 0300 0500
F
-2 0 +1 0 -0.5
Z SM
θ
+90
-90
φ
180°
0°
GEOCENTRIC DISTANCE (Re)

Figure 7

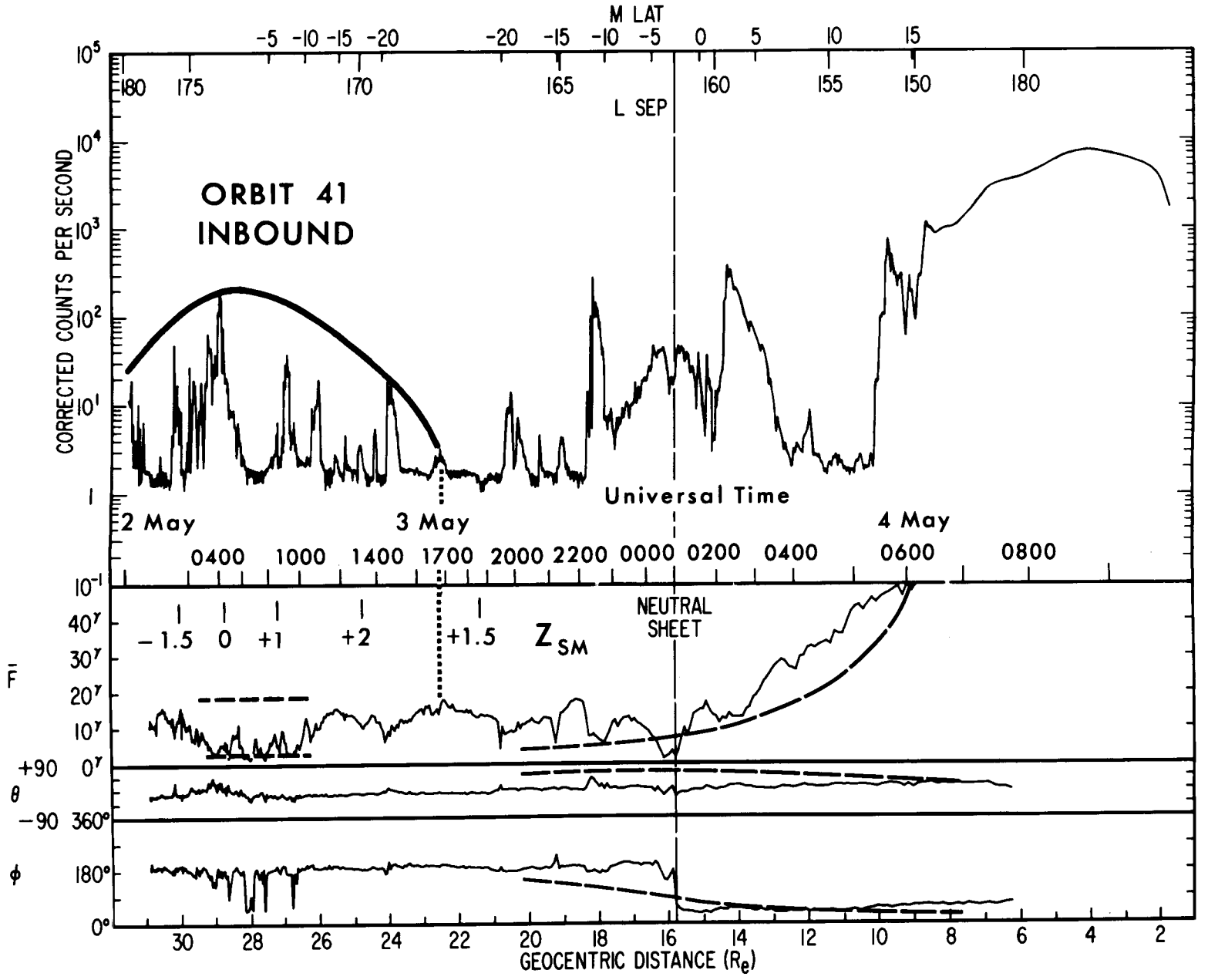
M LAT
-5 -10 -15 -20
-20 -15 -10 -5 0 5 10 15
180 175 170 165 160 155 150 180
L SEP
ORBIT 41
INBOUND
CORRECTED COUNTS PER SECOND
Universal Time
2 May
3 May
4 May
0400 1000 1400 1700 2000 2200 0000 0200 0400 0600 0800
NEUTRAL SHEET
-1.5 0 +1 +2 +1.5
Z_{SM}
F
θ
φ
+90
-90
360°
180°
0°
30 28 26 24 22 20 18 16 14 12 10 8 6 4 2
GEOCENTRIC DISTANCE (R_e)

Figure 8

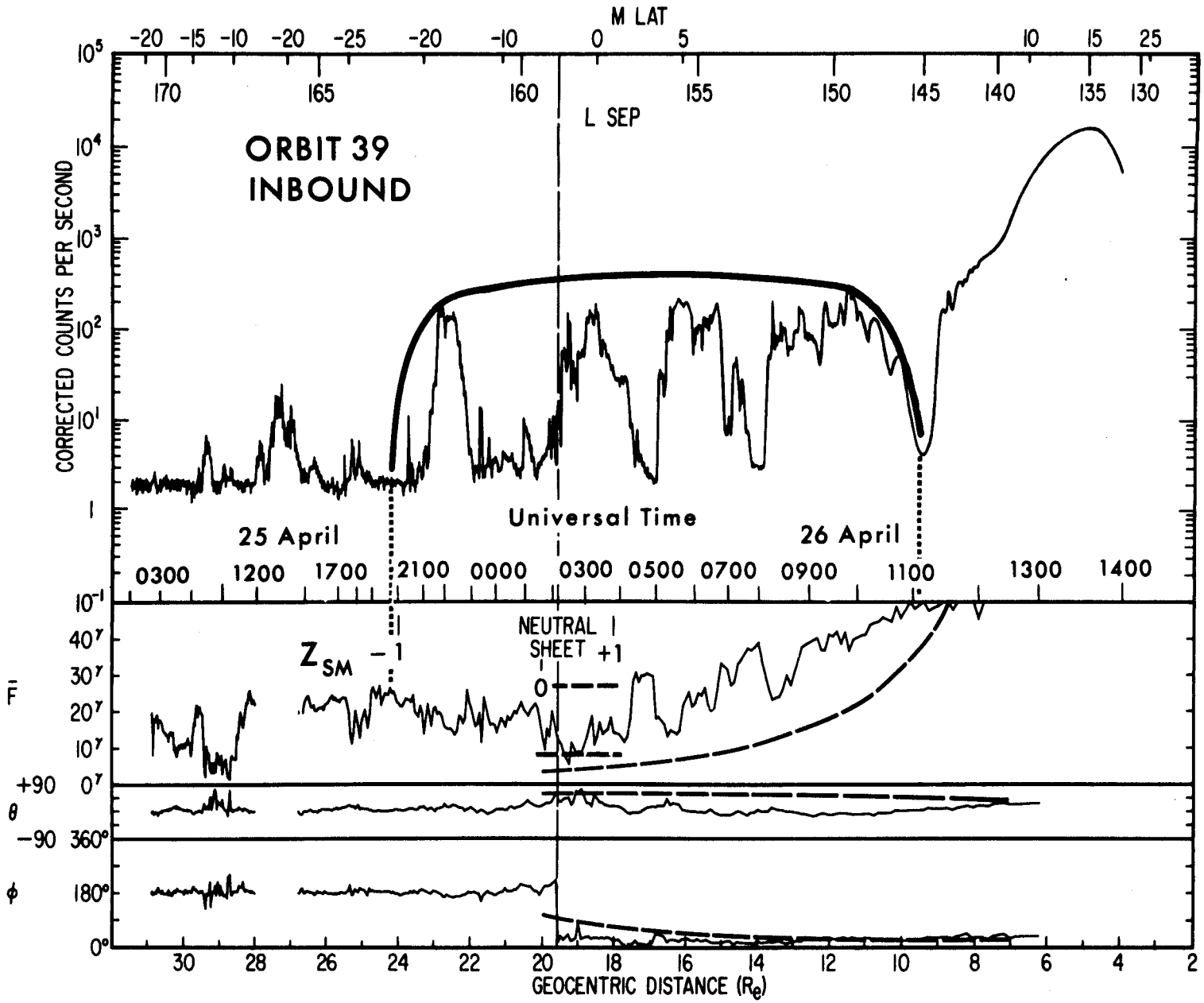
M LAT
-20 -15 -10 -20 -25 -20 -10 0 5 10 15 25
170 165 160 155 150 145 140 135 130
L SEP
ORBIT 39
INBOUND
CORRECTED COUNTS PER SECOND
Universal Time
25 April
26 April
0300 1200 1700 2100 0000 0300 0500 0700 0900 1100 1300 1400
NEUTRAL I
SHEET
Z_{SM}
+1
0
−1
F
θ
+90
−90
φ
360°
180°
0°
GEOCENTRIC DISTANCE (R_e)

Figure 9

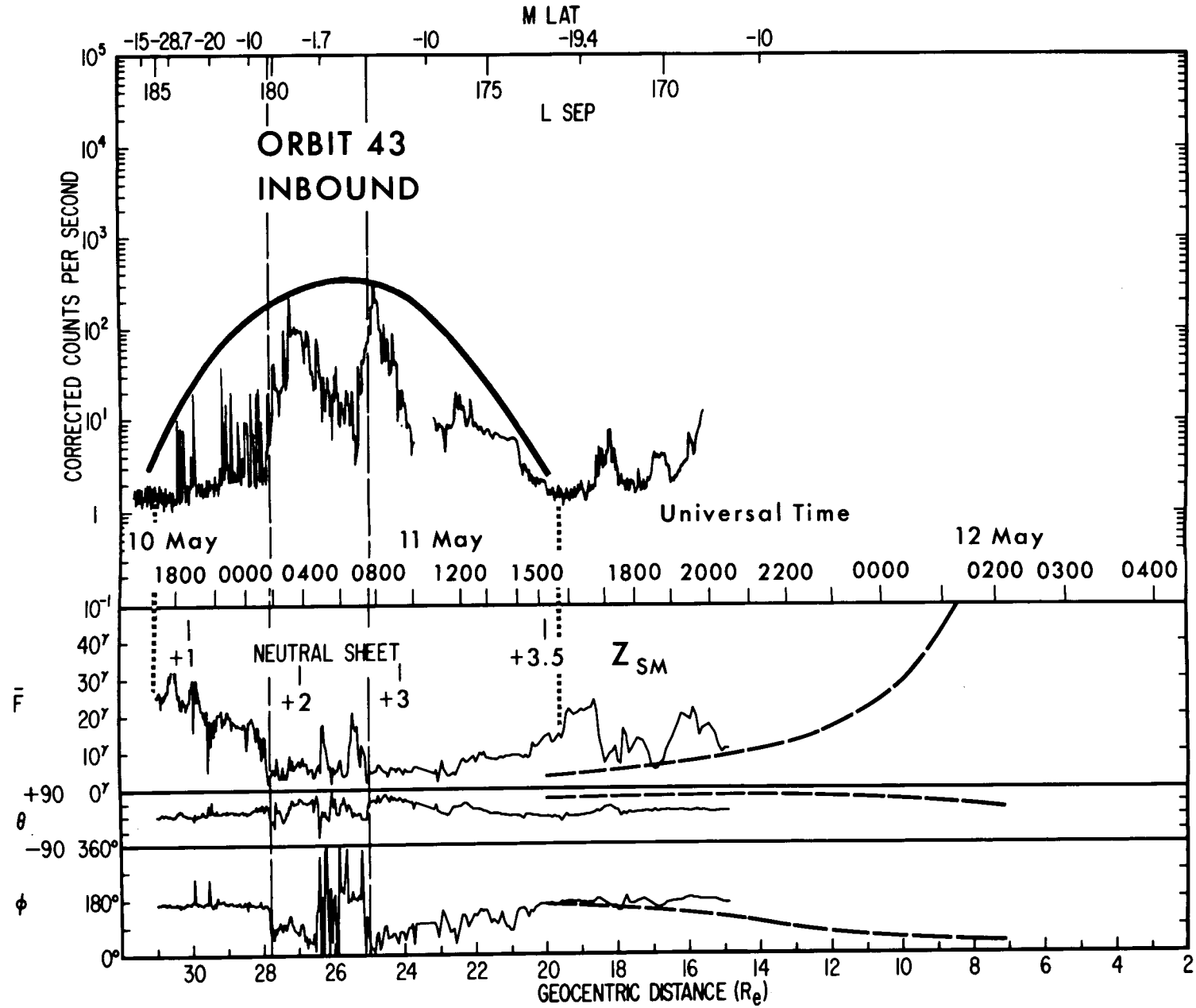
M LAT
-15 -28.7 -20 -10 -1.7 -10 -19.4 -10
185 180 175 170
L SEP
ORBIT 43
INBOUND
CORRECTED COUNTS PER SECOND
Universal Time
10 May
11 May
12 May
1800 0000 0400 0800 1200 1500 1800 2000 2200 0000 0200 0300 0400
+1
NEUTRAL SHEET
+2
+3
+3.5
Z SM
F
θ
φ
+90
-90
360°
180°
0°
30 28 26 24 22 20 18 16 14 12 10 8 6 4 2
GEOCENTRIC DISTANCE (Re)

Figure 10

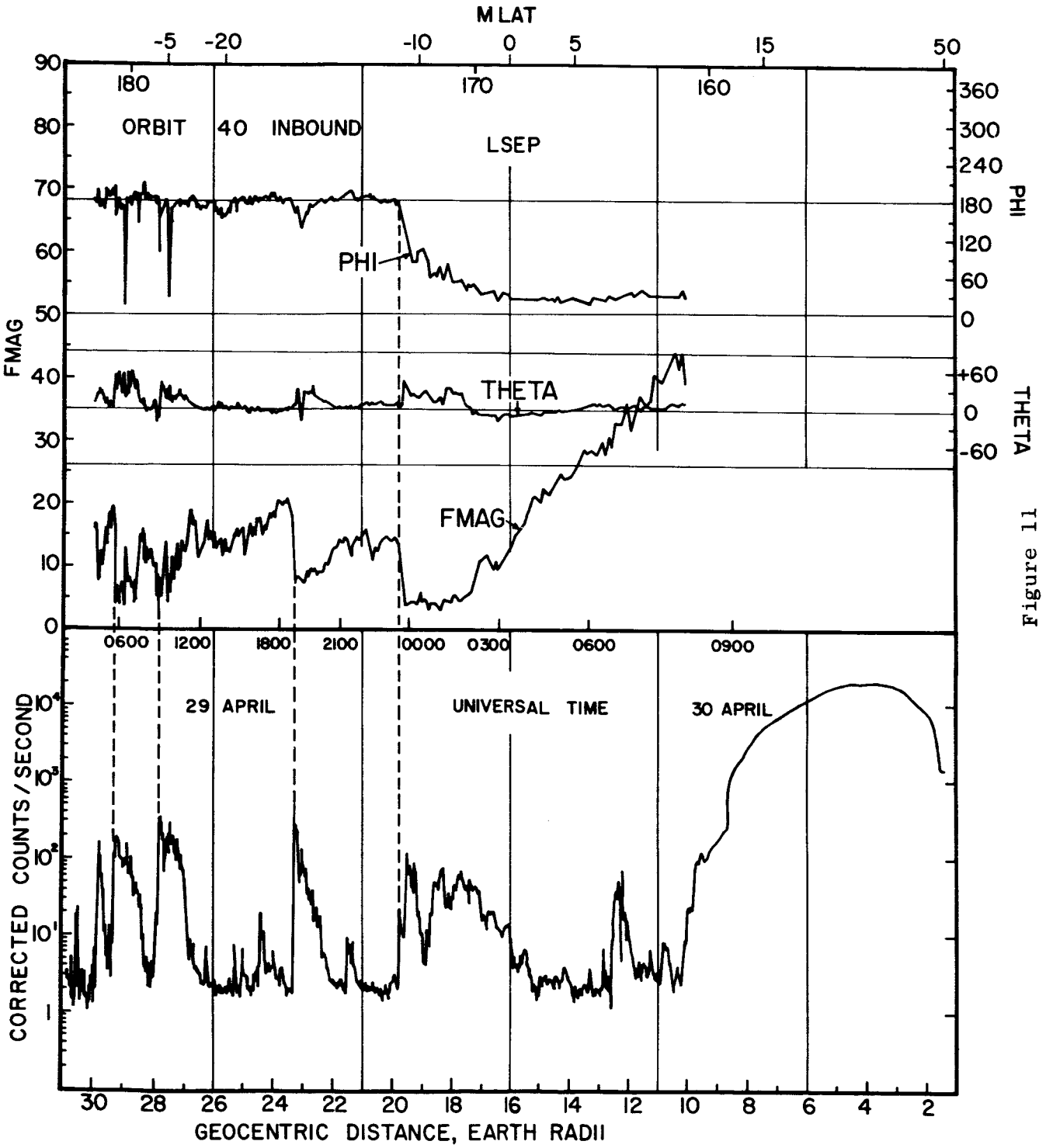
M LAT
-5
-20
-10
0
5
15
50
180
170
160
ORBIT 40 INBOUND
LSEP
PHI
THETA
FMAG
90
80
70
60
50
40
30
20
10
0
360
300
240
180
120
60
0
+60
0
-60
0600
1200
1800
2100
0000
0300
0600
0900
29 APRIL
UNIVERSAL TIME
30 APRIL
CORRECTED COUNTS / SECOND
10^4
10^3
10^2
10^1
1
30
28
26
24
22
20
18
16
14
12
10
8
6
4
2
GEOCENTRIC DISTANCE, EARTH RADII

Figure 11

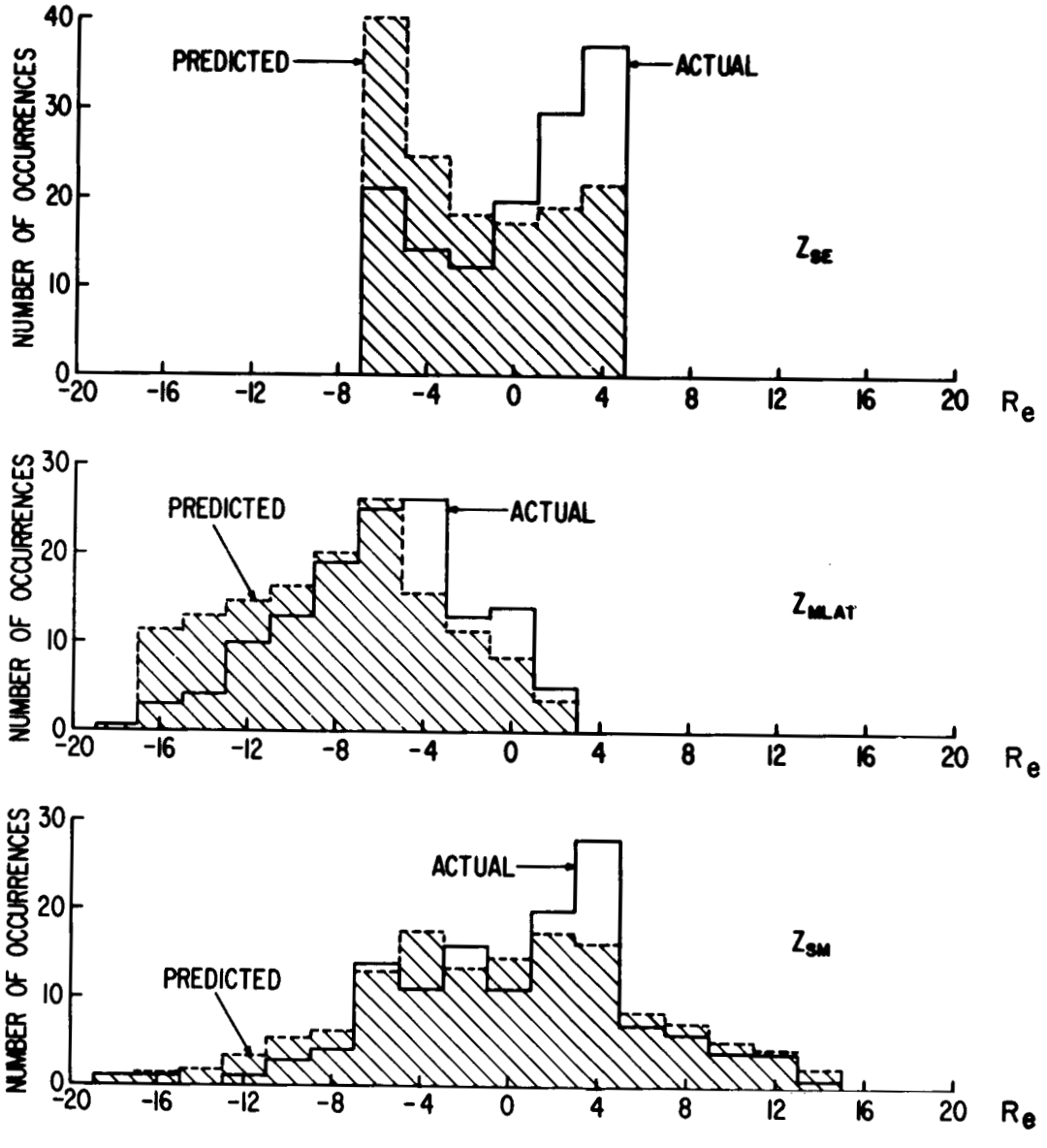
NUMBER OF OCCURRENCES
PREDICTED
ACTUAL
Z_{SE}
R_e
Z_{MLAT}
Z_{SM}
-20
-16
-12
-8
-4
0
4
8
12
16
20
0
10
20
30
40

Figure 12

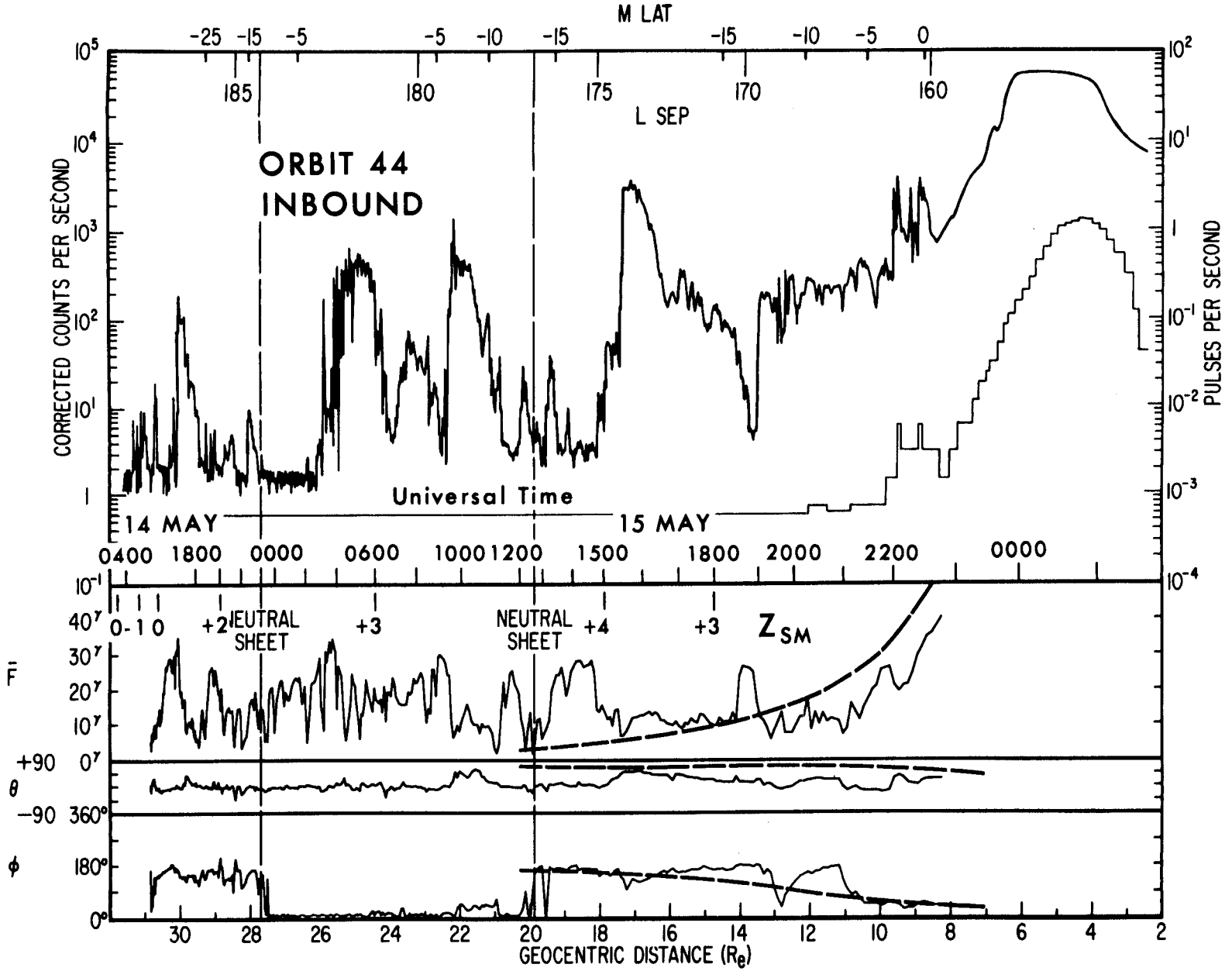
M LAT
-25 -15 -5 -5 -10 -15 -15 -10 -5 0
185 180 175 170 160
L SEP
ORBIT 44
INBOUND
CORRECTED COUNTS PER SECOND
PULSES PER SECOND
Universal Time
14 MAY
15 MAY
0400 1800 0000 0600 1000 1200 1500 1800 2000 2200 0000
0-1 0 +2 NEUTRAL SHEET +3 NEUTRAL SHEET +4 +3
Z_{SM}
F
θ
φ
GEOCENTRIC DISTANCE (R_e)

Figure 13

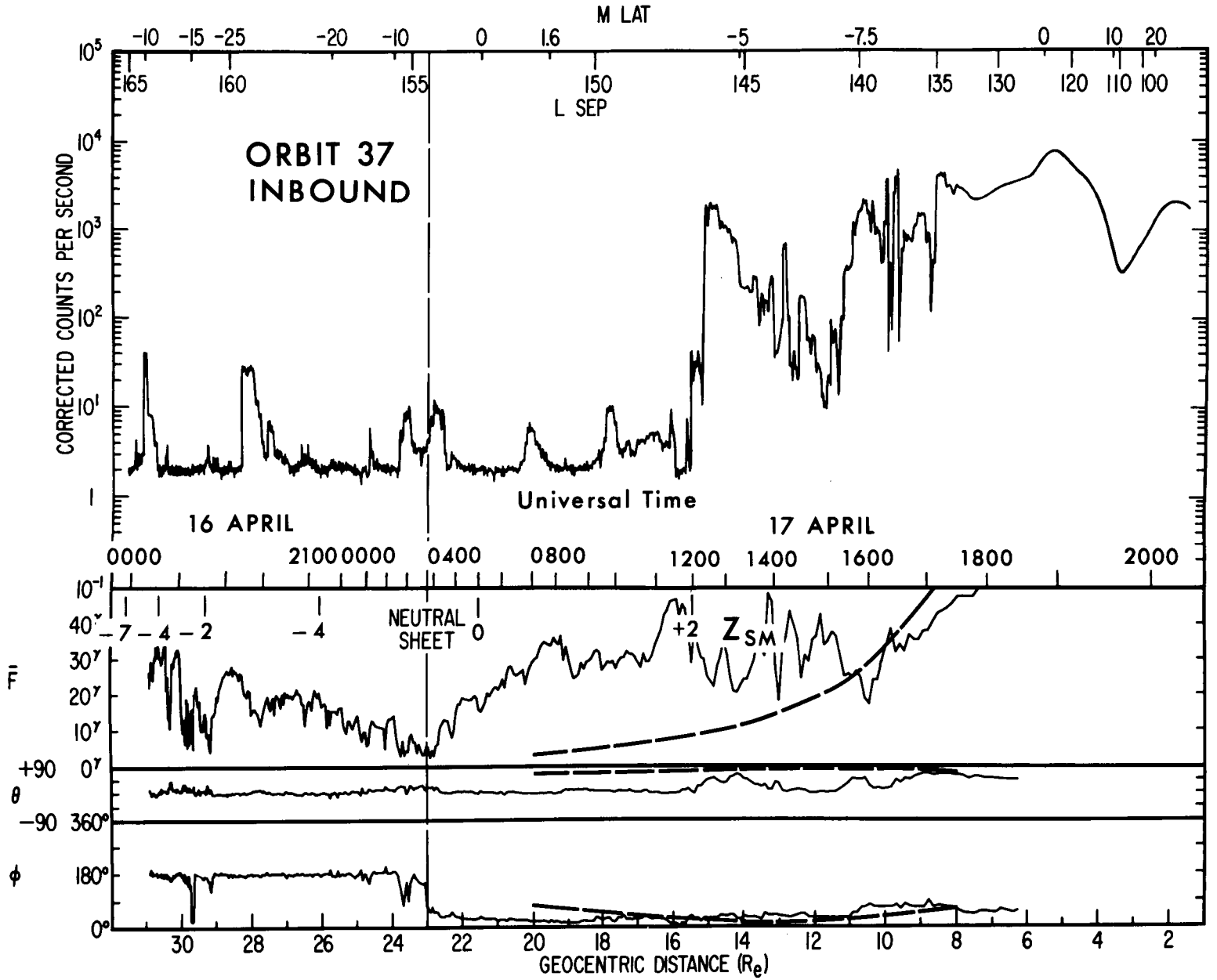
M LAT
-10 -15 -25 -20 -10 0 1.6 -5 -7.5 0 10 20
165 160 155 150 145 140 135 130 120 110 100
L SEP
ORBIT 37
INBOUND
CORRECTED COUNTS PER SECOND
Universal Time
16 APRIL
17 APRIL
0000 2100 0000 0400 0800 1200 1400 1600 1800 2000
NEUTRAL SHEET
-7 -4 -2 -4 0 +2
Z SM
F
θ
φ
+90
-90
360°
180°
0°
30 28 26 24 22 20 18 16 14 12 10 8 6 4 2
GEOCENTRIC DISTANCE (Re)

Figure 14

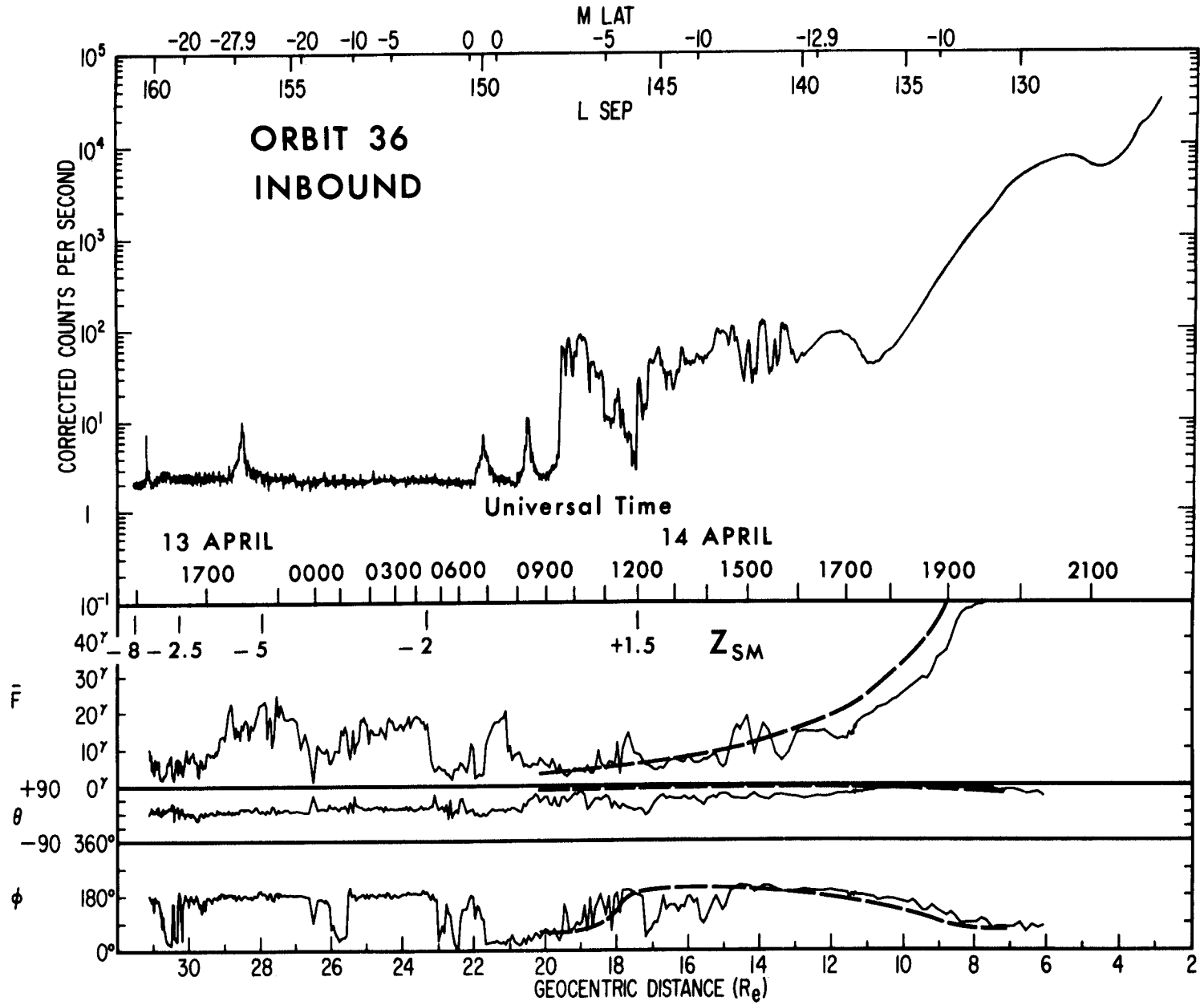
M LAT
-20 -27.9 -20 -10 -5 0 0 -5 -10 -12.9 -10
160 155 150 145 140 135 130
L SEP
ORBIT 36
INBOUND
CORRECTED COUNTS PER SECOND
Universal Time
13 APRIL
14 APRIL
1700 0000 0300 0600 0900 1200 1500 1700 1900 2100
-8 -2.5 -5 -2 +1.5 Z_{SM}
$\bar{F}$
+90
θ
-90
φ
180°
0°
30 28 26 24 22 20 18 16 14 12 10 8 6 4 2
GEOCENTRIC DISTANCE (R_e)

Figure 15

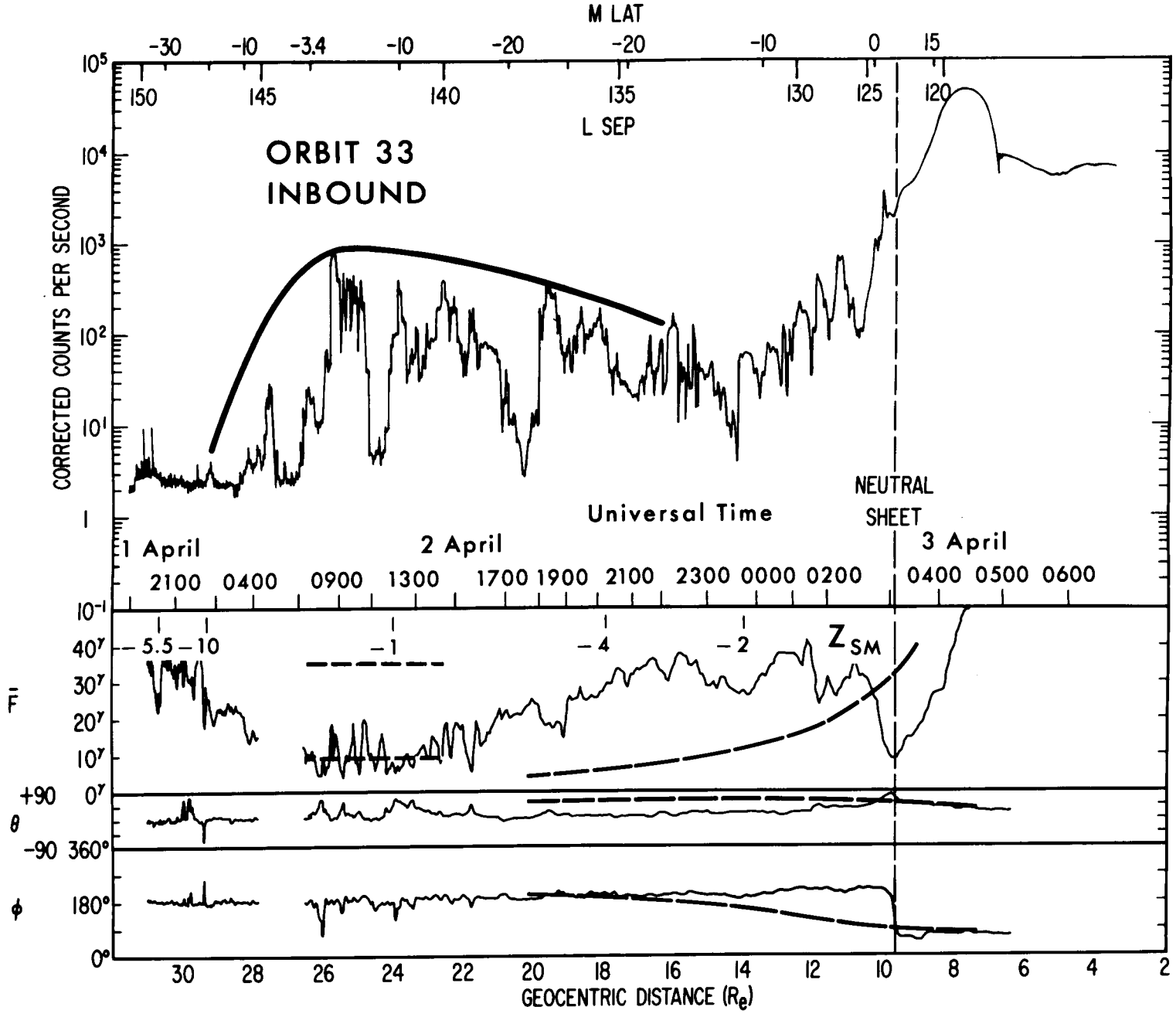
M LAT
-30 -10 -3.4 -10 -20 -20 -10 0 15
150 145 140 135 130 125 120
L SEP
ORBIT 33
INBOUND
CORRECTED COUNTS PER SECOND
Universal Time
NEUTRAL SHEET
1 April
2 April
3 April
2100 0400 0900 1300 1700 1900 2100 2300 0000 0200 0400 0500 0600
-5.5 -10
-1
-4
-2
Z_{SM}
F
θ
φ
+90
-90
360°
180°
GEOCENTRIC DISTANCE (R_e)

Figure 16

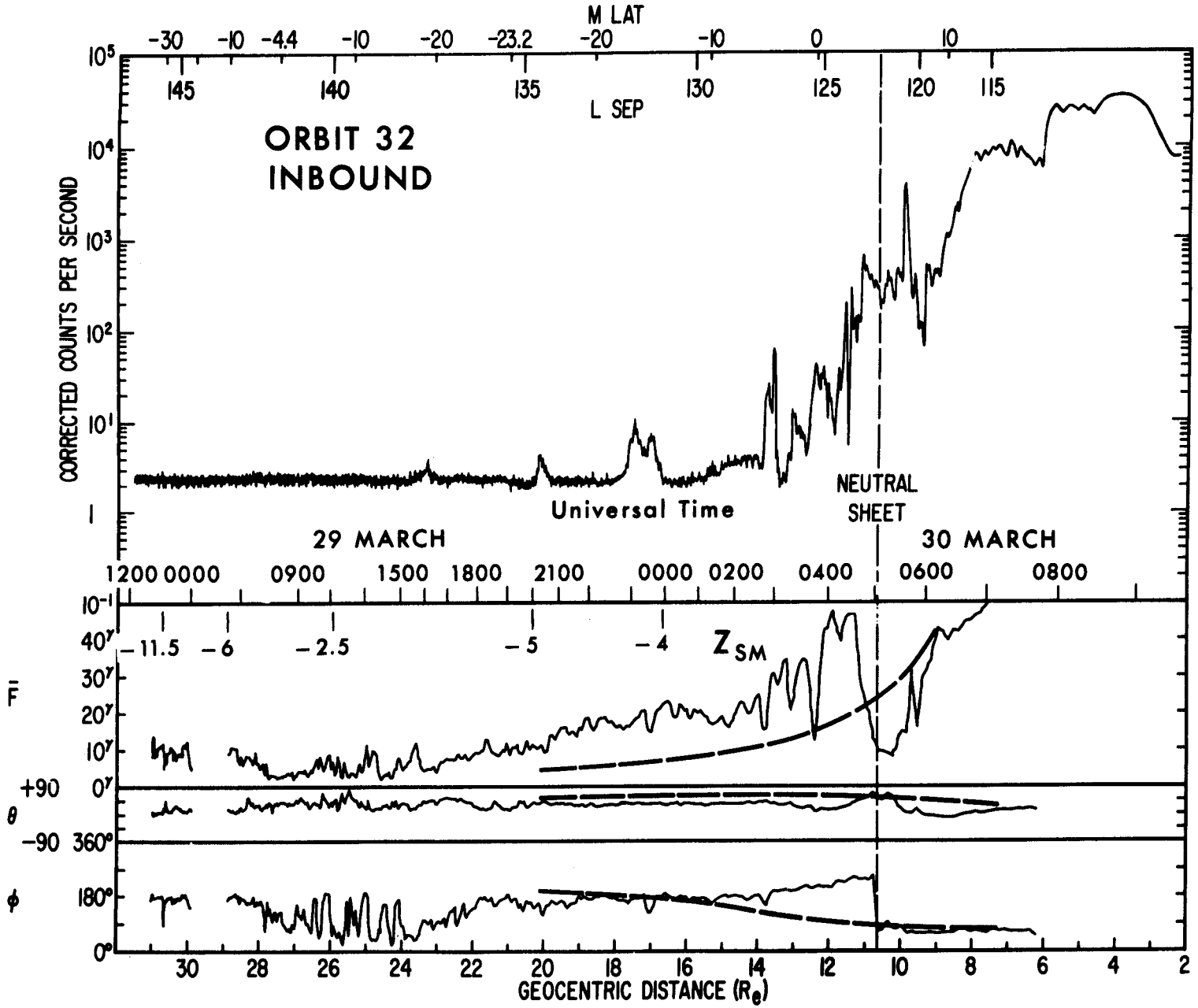
M LAT
-30 -10 -4.4 -10 -20 -23.2 -20 -10 0 10
L SEP
145 140 135 130 125 120 115
ORBIT 32
INBOUND
CORRECTED COUNTS PER SECOND
Universal Time
NEUTRAL SHEET
29 MARCH
30 MARCH
1200 0000 0900 1500 1800 2100 0000 0200 0400 0600 0800
-11.5 -6 -2.5 -5 -4
Z_{SM}
F
θ
φ
+90
-90
360°
180°
GEOCENTRIC DISTANCE (R_e)

Figure 17

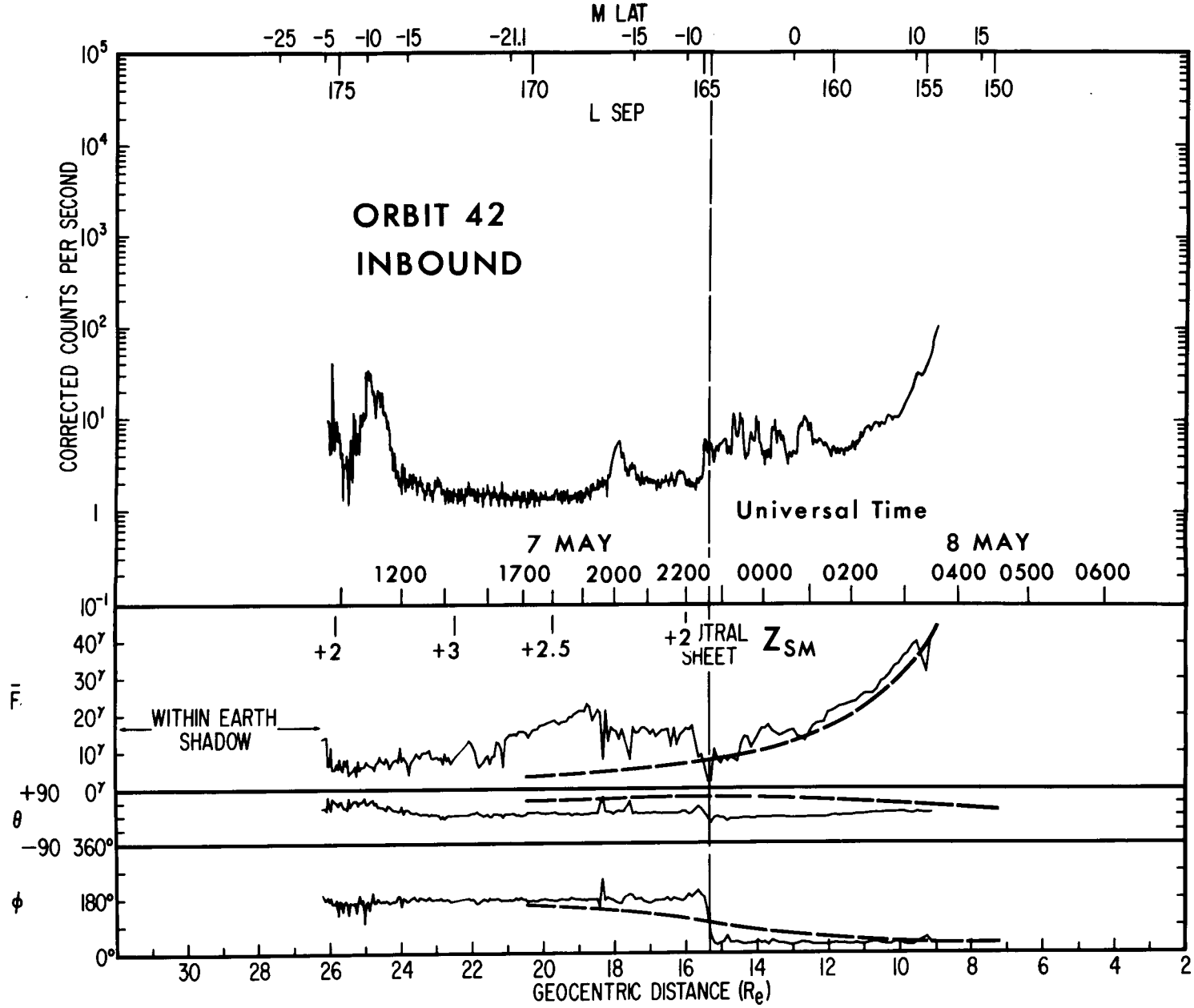
M LAT
-25 -5 -10 -15 -21.1 -15 -10 0 10 15
175 170 165 160 155 150
L SEP
ORBIT 42
INBOUND
CORRECTED COUNTS PER SECOND
Universal Time
7 MAY
8 MAY
1200 1700 2000 2200 0000 0200 0400 0500 0600
+2 +3 +2.5 +2 NEUTRAL SHEET
Z_{SM}
WITHIN EARTH SHADOW
F
θ
φ
+90
−90
360°
180°
0°
GEOCENTRIC DISTANCE (R_e)

Figure 18